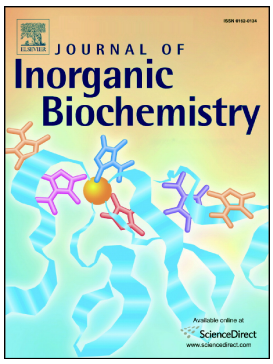

Label-free sensing platform for miRNA-146a based on chromo-fluorogenic pyrophosphate recognition

Anup Pandith, Young Jun Seo

PII: S0162-0134(19)30218-1

DOI: https://doi.org/10.1016/j.jinorgbio.2019.110867

Reference: JIB 110867

To appear in: *Journal of Inorganic Biochemistry*

Received date: 11 April 2019

Revised date: 19 September 2019

Accepted date: 24 September 2019

Please cite this article as: A. Pandith and Y.J. Seo, Label-free sensing platform for miRNA-146a based on chromo-fluorogenic pyrophosphate recognition, *Journal of Inorganic Biochemistry* (2018), https://doi.org/10.1016/j.jinorgbio.2019.110867

Label-Free Sensing Platform for miRNA-146a Based on Chromo-Fluorogenic Pyrophosphate Recognition

Anup Pandith and Young Jun Seo*

Department of Chemistry, Chonbuk National University, Jeonju, 54398, Republic of Korea

Corresponding author: Tel.: +82 63 2703417; fax: +82. 63 2703408

E-mail: yseo@jbnu.ac.kr

Abstract: In this study we applied the dual-responsive chromo-fluorescent Cu^{2+} chelate **1C** for the recognition of miRNA-146a through a pyrophosphate (PPi) sensing strategy in a rolling circle amplification (RCA) process. This approach for the recognition of miRNA-146a was highly robust, selective, and sensitive down to the attomolar (fluorogenic) and sub-micromolar (chromogenic) ranges under modified biochemical conditions at elevated temperature. Probe **1** selectively recognized Cu^{2+} and PPi ions in a sequential manner, as evidenced by colorless→pink→colorless transitions; the fluorescence emissions centered at 480 nm underwent a corresponding *on–off–on* sequence in the bluish-green region. We attribute this reversible switching upon the addition of Cu^{2+}/PPi ions to effective chelation-induced ligand-to-metal charge/electron transfer that resulted in opening of the lactam ring upon complexation and closing of the lactam ring upon decomplexation. We also report a label-free approach for monitoring miRNA-146a amplification in an RCA process under modified T4 ligase and ϕ_{29} buffer conditions, using the Cu^{2+} ensemble **1C** at pH 7.0 (4-(2-hydroxyethyl)piperazine-1-ethanesulfonic acid: HEPES, 10 mM $MgCl_2$); the time required to perform this process (40–50 min) was shorter than conventional RCA process. This ensemble **1C** could recognize miRNA-146a colorimetrically (from pink to colorless) and fluorimetrically ("turn-on" mode) at concentrations within the highly sensitive atto-/nanomolar range under physiological conditions. This cost-effective label-free sensing strategy appears to be a universal method for detecting miRNAs according to the specified length of the template.

Keywords: Chromo-fluorogenic Cu^{2+} ensemble, miRNAs, modified buffers.

Introduction

Label-free optical methods for the identification of genetic materials as vital targets have several advantages over labeling approaches-in particular, higher spatial and temporal resolutions relative to those obtainable using electro-analytical approaches, nuclear magnetic resonance (NMR) spectroscopy, high-performance liquid chromatography (HPLC), and mass spectrometry [1]. Labeling approaches require the synthesis of modified oligonucleotides complimentary to a particular analyte,

with the function based on a Watson–Crick base-pairing mode (duplex) to cause structure-related photophysical changes. Although such processes can have high sensitivities and selectivities, the syntheses can be laborious and time-consuming, and expensive in terms of the chemicals consumed and the highly sophisticated instruments required for characterization [2,3]. Accordingly, in this study we have developed a label-free method to identify miRNAs-short non-coding single-stranded RNA sequences (18-24 nt) in the untranslated region of messenger RNA (mRNAs).

Generally, miRNAs are involved in gene regulation, through induced degradation of mRNA, thereby regulating protein translation. In addition, several miRNAs are also involved in cell proliferation, differentiation, apoptosis, hematopoiesis, and stress resistance, and also play roles in various diseases in humans and animals [3]. A recent investigation revealed that miRNAs are excellent biomarkers-they are stable in serum, plasma, and whole blood lines-and that they exist primarily in encapsulated form in the exosome [4]. Conventional strategies for miRNA sensing rely on a complimentary DNA/RNA (preferably DNA) sequence and fluorophore/quencher, fluorophore (quencher-free), or fluorophore/fluorophore (donor/acceptor pairs for fluorescence resonance energy transfer:FRET) units, in addition to signal amplification techniques [5]. In addition, several miRNA recognition approaches have been developed based on DNA–protein and RNA–protein interactions involving chromofluorescent labels [6]. These strategies typically provide outstanding selectivity toward a specific miRNA under ambient physiological conditions, even in complex biological fluids. In general, the use of labeled oligonucleotides/genetically modified fluorescent proteins requires highly aseptic media, buffers, and dissolved salts (cations or anions) to ensure modulation of the photophysical properties through weak noncovalent interactions-typically, conventional multiple hydrogen bonding (Hoogsteen or Watson–Crick mode), non-classical cation–π, anion–π, NH–π, and OH–π interactions, and van der Waals forces [7]. Exploiting such weak nonspecific interactions could increase the probability of false-positive signals when recognizing low concentrations of miRNA, piRNA (piwi interacting RNA), and mRNA (ca. 10^{-9}–10^{-14} M) in complex biological fluids [8]. To gain high sensitivity and selectivity and allow qualitative analysis, signal amplification methods are required.

Isothermal methods of amplification (rapid amplification kinetics and efficiency) are especially useful for shorter oligonucleotides, including miRNAs; they have several advantages over methods based on the real-time polymerase chain reaction (RT-PCR), northern blotting, or micro arrays [9,10]. Such methods are less destructive toward biomacromolecules, retain the viability of recognition sites, allow variations in the photophysical properties of the fluorophores, and ensure the structural stability of the amplified nucleic acids during the entire process, including the isolation and separation steps [11]. Several isothermal DNA/RNA amplification methods have been developed previously: nucleic acid sequence–based amplification; strand displacement amplification; loop-mediated isothermal amplification; branched DNA, hybrid capture, and DNA cleavage–based signal amplification; the ligase chain reaction; and rolling circle amplification (RCA) [12]. RCA uses a circular template that is generally produced in the presence of the perfectly matched nucleic acid sequence and T4 ligase at ambient temperature. RCA techniques have been applied to identify DNA/RNA with excellent sensitivity (down to attomolar concentrations) and selectivity (1 in 10^6) in complex mixtures.

In this study, we exploited the complexation and decomplexation processes of the hydrazone-based probe **1** (Scheme 1) upon the sequential additions of Cu^{2+} and pyrophosphate (PPi) ions to develop a simple and robust label-free method for the recognition of miRNAs using a convenient RCA process under modified buffer conditions. Several reports describe the identification of PPi ions during nucleic acid amplification processes, mainly relying on PCR [13–15]. Furthermore, various label-free methods have been developed for real-time monitoring using RCA [16–18]. Inspired by those studies, here we initiated a simple and robust label-free method for the recognition of miRNAs in a colorimetric and fluorimetric manner, along with their real-time monitoring.

To establish a simple and handy devise for the nucleic acid chemist to perform isothermal amplification, in this study we investigated some new chromo-fluorogenic techniques. Because of the great significance of miRNA-146a in genetics [21,22], we chose it as the prime target for the RCA process. Herein, we report the highly selective, sensitive, and robust chromo-fluorogenic Cu^{2+}-based ensemble **1C** for the detection of miRNA-146a, along with amplification monitoring with the aid of

PPi ($HP_2O_7^{3-}$) recognition (PPi produced during the RCA process) under modified ligation (T4 ligase)/polymerase (ϕ_{29}) buffer conditions through a *switch-on* response in the blueish-green (**1**) emission channel, as well as a red-to-colorless transition of the solution. We also describe a simple formulation for modification of the T4 ligation and ϕ_{29} buffer to improve the sensitivity of miRNA detection in terms of the PPi produced through the enzymatic isothermal amplification process under physiological conditions. To the best of our knowledge, colorimetric and fluorimetric methods for miRNA-146a recognition, performed using a PPi sensing platform involving enzymatic isothermal amplification of nucleic acids under modified buffer conditions, have not been reported previously.

Experimental Section

General Materials and Methods

^{1}H and ^{13}C NMR spectra were recorded using a Bruker AM-400 spectrometer. UV–Vis absorption spectra were recorded using a Shimadzu UV-1650PC spectrophotometer. Fluorescence spectra were recorded using a JASCO FP-6500 fluorescence spectrometer (equipped with a Xe discharge lamp) and 1-cm quartz cells, with an excitation and emission slit width of 1/10 nm (readings obtained in 96-well plates). All optical measurements were performed at 25 °C. Solutions of the probe **1** were prepared, stored, and analyzed in the dark, and special care *(always using freshly prepared solutions and avoiding exposure to sunlight)* was taken during analysis. Analytical-grade ethanol (EtOH) and acetonitrile (MeCN) were purchased from Merck. Tris (hydroxymethyl)aminomethane), HEPES, metal salts (perchlorate/chloride), and anions (tetrabutylammonium/sodium salt) were purchased from Sigma-Aldrich and used as received. Fluorescence quantum yields were determined by integrating the corrected fluorescence spectra. 9,10-Diphenylanthracene in *n*-heptane was used as the fluorescent standard (φ = 0.84) for correcting all fluorescence spectra. The fluorescence spectra were recorded immediately after sample preparation. The probe **1** and its solutions were stored in the dark prior to use. Association constants were calculated through non-linear fitting of the UV–Vis and fluorescence spectroscopic data, using the ExpDec equation (non-linear fitting, where $K = t$) in *Origin.8* (professional) software. The values obtained from plotting the respective absorption/emission signal intensities with respect to the concentration of Cu^{2+}/PPi furnished the values of K (1:1)/K_1 and K_2 (1:2).

Upon obtaining the values of K/K_1,K_2 (average), the binding strengths of the interactions of the analytes with the probe were calculated. Details of the calculation methods are provided in the Supplementary Materials.

All-natural oligonucleotides (5´-P-padlock probe, miRNAs) were purchased from Bioneer (Seoul, Republic of Korea). Deoxyribonucleotide triphosphates mixture 2 mM each (dNTPs), T4 DNA ligase (400 U/μL), T4 ligase buffer, ϕ_{29} DNA polymerase (10 U/μL), EXO-I (20 U/μL), EXO-I buffer (1x), and ϕ_{29} DNA polymerase (10 U/μL) were purchased from Enzynomics (Bioneer, Republic of Korea). The 10x ϕ_{29} buffer was formulated to 400 mM Tris-HCl, 500 mM $MgCl_2$, 500 mM KCl, and 500 mM $(NH_4)_2SO_4$ [23, 24]. The ligation reaction was performed using 20 μL of a reaction mixture containing 1x ligation buffer [10x buffer containing 500 mM Tris-HCl, pH 7.5, 100 mM $MgCl_2$, 100 mM KCl, 100 mM $(NH_4)_2SO_4$, 10 mM ATP]. Prior to adding T4 DNA ligase and the ligation buffer, the oligonucleotide mixture was denatured at 85 °C for 2 min, then cooled slowly to room temperature over 10–15 min. After annealing, T4 DNA ligase and the ligation buffer were added to the mixture, which was then incubated at 37 °C for 3-5 h [25]. The stop solutions (ca. pH 4 quick deactivation of ϕ_{29}, avoiding optical fluctuations) were additionally supplemented with Cu^{2+} ions (approximately one equivalent with respect to PPi produced in the ligation step) in accord with the amount of circular template that was taken for the RCA process. The stop solution containing a combination of 95% formamide/MeCN (pH 4.0, 5 μL) enhanced the sensitivity in the supernatant, which was easier to handle with minimal fluctuations in optical signals.

All oligonucleotides (including the padlock probe) were dissolved and diluted to a certain concentration in TRIZMA (Tris-HCl supplemented with 10 mM $MgCl_2$ and 50 mM NaCl) buffer; respective miRNAs were diluted in DEPC buffer [diethyl pyrocarbonate in autoclaved deionized (DI) H_2O] and stored at 4 °C prior to use. DI water (resistance: >17.97 MΩ·cm) was used for all of the biochemical reactions. The concentrations of the respective oligonucleotides are represented herein as single-stranded concentrations; they were calculated by measuring the absorbance at a wavelength of 260 nm. Molar extinction coefficients were determined using the software Oligo-analyzer 3.1 (available at http://sg.idtdna.com/calc/analyzer).

Gel Electrophoresis

Native polyacrylamide gel electrophoresis (nPAGE, 18%) was adopted to characterize the DNA products. The reaction mixture (10 μL) was mixed with 6x loading buffer (2.5 μL) and loaded into the well. Gel electrophoresis was performed in 1x TBE buffer (89 mM Tris, 89 mM borate, 2 mM EDTA, pH 8.3) at a constant potential of 95/80 V for 90–180 min and a current of 3 mA, followed by scanning on a gel image system. Similarly, RCA products (15 μL) were mixed with the loading buffer (6x, 2.5 μL) and run with 2% agarose gel for 40/60 min (100/50 V) in 1x TBE buffer. The gel was stained with ethidium bromide (EB) and then photographed using a ChemiDoc MP imaging system (Bio-Rad).

Synthesis of Probe and Cu^{2+} Ensembles

Probe 1 and 1●Cu^{2+} Ensemble: Rhodamine hydrazide (250 mg, 0.550 mmol) and 4-(diethylamino)salicylaldehyde (106 mg, 0.550 mmol) were mixed in absolute EtOH (13 mL) and stirred at 82 °C for 4 h under a N_2 atmosphere in the presence of a catalytic amount of trifluoroacetic acid (TFA). The solvent was evaporated under reduced pressure and the residue purified through column chromatography (eluent: hexane/CH_2Cl_2/MeOH/EtOAc/NH_4OH, 2:3:1:3.5:0.5), affording **1** as a yellowish-white solid (320 mg, 91% yield); ^{1}H NMR (400 MHz, $CDCl_3$) δ 1.09–1.17 (m, 18H), 3.29–3.41 (m, 12H), 6.09–6.13 (m, 2H), 6.23–6.26 (m, 2H), 6.45–6.50 (m, 4H), 6.92 (d, 1H), 7.14–7.17 (m, 1H), 7.47–7.50 (m, 2H), 7.93–7.95 (m, 1H), 9.18 (s, 1H), 10.94 (s, 1H); ^{13}C NMR (100 MHz, $CDCl_3$) δ 12.6, 12.7, 44.3, 44.5, 66.5, 97.9, 98.3, 103.3, 105.9, 107.5, 108.0, 123.0, 124.0, 128.1, 128.4, 130.9, 132.8, 148.9, 150.4, 150.6, 153.7, 154.7, 160.6, 163.6; High-resolution fast atom bombardment mass spectrometry (HR-FAB MS): $[C_{39}H_{46}N_5O_3]^+$ calcd *m*/*z* 632.3601, found 632.3598. Fourier transform infrared (FTIR) spectroscopy (KBr, cm^{-1}): 3454 (br), 2967, 1695, 1631, 1517, 1303, 1132. The **1**●Cu^{2+} (1:1) ensemble was prepared by mixing **1** (50 mg, 0.080 mmol) and $CuCl_2$ (13.5 mg, 0.080 mmol) in MeCN in the dark under a N_2 atmosphere, furnishing a dark-pink solid (56 mg, 97%); HR-FAB MS: calcd *m*/*z* 727.2350, found 727.2353; FTIR (KBr, cm^{-1}): 3450, 2970, 1600, 1588, 1465, 1354, 1147.

Results and Discussion

Considering the cost, the redox capabilities of divalent copper in the biological window, and the superiority of copper over other transition metals in terms of toxicity and biocompatibility [25], for this study we designed a highly selective Cu^{2+} ensemble (**1C**) capable of "*switch-on*" responses towards PPi. After photophysical studies of the excited states of various chromo-fluorescent materials, we found that only a few fluorophores with selected functionality exhibited the peculiar variations in excited state upon complexation with Cu^{2+} ions under specified conditions. Ideally, our probe should detect Cu^{2+} and PPi ions in both a sequential manner and a reversible manner to avoid interference and false-positive signals. To simplify the synthesis and obtain a highly efficient hydrazone-based probe having a small-molecule architecture, we prepared **1** for the selective recognition of Cu^{2+} and PPi ions in a chromo-fluorogenic manner under physiological conditions. With the aid of the PPi generated during isothermal signal amplification through the consumption of dNTPs in RCA, this probe **1C** allowed us to recognize miRNA-146a using both colorimetric and fluorimetric methods under physiological conditions. In addition, to avoid interference from thiols [e.g., dithiothreitol (DTT), a prime chemical component in the commercially supplied T4 ligase and ϕ_{29} buffer; it functions as an enzyme stabilizer (inhibition of aggregation and oxidation via S–S intramolecular cysteine bonding during storage)], we implemented a new buffer formulation with minor modifications [26]. Accordingly, we identified the most suitable elevated temperature, enzymes, and amount of the padlock probe to ensure a robust isothermal amplification process.

(Scheme 1 will be added here)

We prepared the probe **1** and characterized it using NMR spectroscopy and mass spectrometry (see ESI for details). Initially, we examined the fluorescent probe **1** using UV–Vis and fluorescence spectroscopy to evaluate its sensing capabilities toward Cu^{2+} and PPi ions under physiological conditions. By considering nucleic acids as prime analytes, we initiated the UV–Vis spectral studies of the probe **1** using HEPES buffer at pH 7.0 in the presence of 10 mM of $MgCl_2$ as a prime salt. To ensure effective and precise stoichiometric analyses, we performed our optical studies

in MeCN/H_2O (3:7, v/v%), where the H_2O (pH 7.0) fraction included HEPES and 10 mM $MgCl_2$. Because of its unusual electronic absorption and emission behavior (blue-green), the bichromophoric system of (colorless) rhodamine and *N*,*N*-diethylaminosalicylaldehyde fluorophores, connected through a hydrazone linkage, functions as a colorimetric (mainly from the rhodamine unit) and fluorogenic (salicylaldehyde unit) system toward soft metals and bases [27].

A 25 μM solution of the probe **1** in MeCN/H_2O (3:7, v/v%) provided absorption maxima at (λ_{max}) 383, 321, and 277 nm, due to the symmetry-forbidden and photochemically allowed $\pi\rightarrow\pi^*$ and $n\rightarrow\pi^*$ transitions (Fig. 1a). The higher-energy transitions were associated with $S_0\rightarrow S_2$ transitions of the xanthene unit of the rhodamine backbone. Upon addition (10.0 eq.) of the perchlorate salts of K^+, Na^+, Li^+, Ca^{2+}, Mg^{2+}, Rb^+, Co^{2+}, Ni^{2+}, Fe^{2+}, Zn^{2+}, Pb^{2+}, Cu^{2+}, Hg^{2+}, Al^{3+}, Ga^{3+}, Fe^{3+}, and In^{3+}, only Cu^{2+} induced a dramatic color change from light-yellow to pink in the HEPES buffer solution, with a characteristic new band appearing at 558 nm (log ε = 4.5705) with a broad shoulder at 519 nm (log ε = 4.1219) and an isosbestic point at 388 nm. In contrast, the absorptivities at 277 nm (log ε = 4.2553) and 321 nm (log ε = 4.0763) decreased; the signal at 383 nm (log ε = 4.3972) was red-shifted to 399 nm (log ε = 4.3344) with a prominent decrement in absorptivity, suggesting the formation of an open form of the hydrazone linkage of the rhodamine-diethylaminosalicylaldehyde units involved in the Cu^{2+} chelation process. The significant changes were observed approximately 20 min after the addition of 1.0 eq. of Cu^{2+} ions (Fig. S1), suggesting a Cu^{2+}-induced spirolactam ring opening process. A Job's plot revealed the formation of a 1:1 complex, as evidenced by the maximum absorptivity appearing at a mole fraction of 0.5 (Cu^{2+}) with respect to **1** (Fig. S2). UV–Vis spectroscopic titration of **1** with Cu^{2+} ions revealed an appreciable association constant ($K_a = 4.91 \times 10^4\ M^{-1}$) upon fitting the data at 558 nm (Fig. S3).

(Figure 1 will be added here)

Next, we used a displacement approach to identify the stability of the Cu^{2+} complex **1**●Cu^{2+} (1:1, **1C**) in the presence of various biologically relevant anions (25.0 eq.) as tetrabutylammonium salts: I^-, Br^-, Cl^-, F^-, NO_3^-, ClO_4^-, $H_2PO_4^-$, PPi, $SO_4^{2-}(Na^+)$, HSO_4^-, CO_3^{2-}, PO_4^{3-}, and AcO^-; here, only PPi extruded the Cu^{2+} ions selectively, as evidenced by changing the red-colored solution to colorless (Fig. 1b). The decrease in the intensity of the signal at 558 nm and the increase in intensity at 383 nm, resulting in revival of the UV–Vis spectral electronic transitions of probe **1**, confirmed the formation of a stable free $[Cu^{II}(P_2O_7)_2(H_2O)_n(MeCN)_{6-n}]^{6-}$ complex.

In addition to these biologically relevant ions, we also investigated the effects of 50.0 eq. (in excess to evaluate potential optical interference) of the sodium salt of adenosine monophosphate (AMP), adenosine diphosphate (ADP), various dNTPs (dATP, dGTP, dCTP, and dTTP; 2 mM each), the 15-nt adenine oligonucleotide A-15, bovine serum albumin (BSA), and RNA (isolated) toward **1C**; none elicited any response from the red-colored solution of the metal ensemble **1C**, suggesting negligible interference from nucleic acids, proteins, and tri- and mono-phosphates (Fig. S4). UV–Vis spectroscopic titration of the 25 μM Cu^{2+} ensemble of the probe **1** with PPi ions (Fig. S5) revealed a very high binding constant ($K_a = 2.88 \times 10^5\ M^{-1}$), based on 1:2 binding stoichiometric calculations. Thus, our rationally designed probe **1** performed the sequential recognition of Cu^{2+} and PPi ions in a colorimetric manner, aided through complexation and decomplexation processes under physiological conditions.

In general, nucleic acid recognition, isolation, and chemical modification are performed predominantly in aqueous (buffered) solutions with MeCN as a co-solvent. Gratifyingly, we found that the sensing capabilities of **1** for the sequential recognition of Cu^{2+} and PPi ions were very effective in buffered $MeCN/H_2O$ (3:7, v/v%).

Upon excitation at 402 nm, the emission spectra of the probe **1** featured a peak near 480 nm (ϕ = 0.135) with broadened features, suggesting that this signal resulted from the diethylaminosalicylaldehyde hydrazone unit. The spectra also validated the "turn-off" nature of the rhodamine unit (red emission), which existed in the lactone state at neutral pH (HEPES buffer) in the

presence of MeCN as a co-solvent. Excitation at 550–560 nm did not induce any characteristic rhodamine emission; time-resolved fluorescence decay measurements supported the dominant characteristics of one of the fluorophores in the dual-fluorophore chromo-fluorogenic material (Figs. S6a and S6b). Upon addition of 10.0 eq. of the cations K^+, Na^+, Li^+, Cs^+, Ca^{2+}, Mg^{2+}, Rb^+, Co^{2+}, Ni^{2+}, Fe^{2+}, Zn^{2+}, Pb^{2+}, Cu^{2+}, Hg^{2+}, Al^{3+}, Ga^{3+}, Fe^{3+}, and In^{3+}, only Cu^{2+} induced quenching (ϕ = 0.021) by greater than 90%, centered at (λ_{em}) 480 nm, within 15-20 min (Fig. 2a). A Job's plot of the fluorescence data confirmed a 1:1 binding stoichiometry between Cu^{2+} and **1** under physiological conditions (Fig. 2b).

Fluorescence titration at (λ_{em}) 480 nm and non-linear regression provided a value of K_a for the interaction between **1** and Cu^{2+} of 6.40×10^5 M^{-1}, with a good regression coefficient (Fig. S7). HR-FAB MS revealed a peak at *m*/*z* 727.2353, confirming the formation of a 1:1 **1**●Cu^{2+} (**1C**) complex (calcd: *m*/*z* 727.2350) (Fig. S8). Fourier transform infrared spectroscopy (FTIR) spectroscopy revealed peaks at 3454, 2967, 1695, 1631, 1517, 1303, and 1132 cm^{-1} for **1** and at 3450, 2970, 1600, 1588, 1465, 1354, and 1147 cm^{-1} for the complex **1C** (Fig. S9).

(Figure 2 will be added here)

We calculated the energy-minimized structure of **1C** through density functional theory (DFT), using the ωb97X-V/6-311+G(2df,p) basis set in H_2O as an implicit medium (Fig. 3). Coordinate bonds existed between the Cu^{2+} center and the phenolate oxygen atom ($O^-\cdots Cu^{2+}$, 1.91 Å), the nitrogen atom of the hydrazone unit ($CO\text{-}N^-\cdots Cu^{2+}$, 1.93 Å), and the oxygen atom of the hydrazide unit ($HNC\text{-}O^-\cdots Cu^{2+}$, 1.92 Å), characterizing a square-planar geometry for the complex (Fig. 3a). The distributions of the highest occupied molecular orbitals (HOMOs) and lowest unoccupied molecular orbitals (LUMOs) for **1** were located on the *N*,*N*-diethylaminosalicylaldehyde hydrazone unit and the hydrazide linkage, respectively, but they switched predominantly to the rhodamine unit in **1C**. The

band gap energies ($\Delta E = E_{HOMO} - E_{LUMO}$) of **1** and **1C** were –3.21 and –2.29 eV, respectively, consistent with the UV–Vis spectroscopically determined electronic transitions (Fig. 3b).

In the excited state geometry of **1C**, the HOMO and LUMO distributions were located predominantly on the chelation part, consistent with strong electron transfer accompanied by effective d→π electronic coupling through a paramagnetic Cu^{2+} species (Fig. S10). The different electronic distributions in the ground and excited state geometries of **1** and **1C** validated the existence of strong electronic coupling between the rhodamine and diethylaminosalicylaldehyde units through the Cu^{2+} ions only upon complexation. In addition, photoinduced electron transfer (PET) was enhanced from the Cu^{2+} ions to the rhodamine (photo-oxidized) unit through the diethylaminosalicylaldehyde unit [$d_{Cu2+}\rightarrow(\pi)_{DSA}\rightarrow(\pi)_{Rh}$]; this process was the main reason for quenching upon excitation at 402 nm. The existence of such paramagnetic behavior in organic units was also evidenced through hyperfine splitting in electron spin resonance (ESR) spectra (Fig. S11). Thus, we speculate that the probe **1** was capable of recognizing Cu^{2+} ions through opening of the lactam ring (visualized through a pink color), accompanied by PET-based quenching in the green channel upon excitation at 402 nm.

(Fig. 3 will be added here)

Next, we used 1 μM of the ensemble 1:1 stoichiometric complex **1C** for fluorescence studies with the anions (25.0 eq.) I^-, Br^-, Cl^-, F^-, NO_3^-, ClO_4^-, $H_2PO_4^-$, PPi, $SO_4^{2-}(Na^+)$, HSO_4^-, CO_3^{2-}, PO_4^{3-}, and AcO^-; only PPi extruded the Cu^{2+} ions selectively, with a "switch-on" of the signal centered at 480 nm (Fig. 4). The association constant ($K_a = 2.86 \times 10^6\ M^{-1}$), obtained through nonlinear curve fitting of the fluorescence titration data, confirmed that the decomplexation process (Figs. 5c, 5d, and S12) was more feasible than the complexation process (Figs. 5a, 5b, and S7). The electrospray ionization (ESI) mass spectrum of the in situ–generated ensemble featured a peak at *m*/*z* 488.7000, suggesting the successful displacement of Cu^{2+} ions from **1C** (Fig. S13). Other biologically relevant species, namely dNTPs, A-15 (ssDNA), AT-15 (dsDNA), BSA, RNA (miRNA-146a), T4 ligase, ϕ_{29} polymerase, ϕ_{29} buffer, KCl, NH_4Cl, $MgCl_2$, and PO_4^{3-}, induced no significant changes to the Cu^{2+}

ensemble, confirming that the designed probe **1** was suitable for both colorimetric and fluorimetric in vitro diagnostic tests (Figs. S14 and S15).

(Fig. 4 will be added here)

We employed pH-dependent UV–Vis and fluorescence spectroscopy to determine that the probe **1** could be used to recognize Cu^{2+} and PPi ions from pH 3 to 11 in a sequential manner (Fig. S16). Notably, glutathione (glut), cysteine (cyst), homocysteine (Hcyst), free sulfides (H_2S), and biologically relevant H_2O_2 species (i.e., $O_2^{\bullet}$) had some significant effects, providing changes in color from pink to pale-pink in the absorption spectra and with partial revival of fluorescence (Fig. S17). Amino acids not containing thiol units did not induce any significant changes in the optical behavior (Fig. S18). The lowest chromo-fluorogenic responses toward the Cu^{2+} and PPi ions were in the nanomolar and femtomolar ranges under physiological conditions, confirming the high sensitivity of this system toward the respective analytes (Figs. S19 and S20).

(Figure 5 will be added here)

^{1}H NMR spectra (Fig. 6) of the probe **1** (1.5×10^{-3} M) in CD_3CN/D_2O (7:3, v/v%) revealed broadening of the resonances, without any substantial shifts, upon addition of 1.0 eq. of paramagnetic Cu^{2+} ions. Sequential addition of the sodium salt of PPi led to the reappearance of the resonances of **1** in the mixed aqueous medium. Minor shifts in the signals of the up-field aromatic protons of **1** were due to the increased ionic strength upon addition of the PPi ions to the deuterated solvent. Thus, sequential *on–off–on* switching occurred upon sequential addition of Cu^{2+} and PPi ions in a reversible manner.

(Figure 6 will be added here)

The electron paramagnetic resonance (EPR) spectrum of **1C** featured signals at 3120, 3190, 3270, 3320, 3350, and 3390 G (superfine splitting), consistent with Cu^{2+} ions (with values of *g* from

approximately 2.20 to 2.03) bound to probe **1** (Fig. 7; Table ES1). The presence of two positive peaks, as well as both positive and negative peaks, validated the existence of an organic radical associated with a Cu^{2+} ion. In contrast, addition of three equivalents of PPi ions led to peaks appearing at 3090 and 3220 G, similar to the characteristic bands of the $Cu(PPi)_2$ complex [28-30]. In contrast, under similar conditions, the spectrum of the probe **1** did not feature any peaks in the region 3000-4000, confirming that organic radicals accompanied by paramagnetic Cu^{2+} were present only in the solution of **1C**. Thus, our UV–Vis, fluorescence, NMR, and ESR spectra were all consistent with the Cu^{2+} ions being displaced from **1C** upon the addition of PPi ions under neutral conditions, rather than the formation of any associative-type complex.

(Figure 7 will be added here)

We attribute the binding phenomenon of **1** with Cu^{2+} ions, accompanied by strong metal→ligand charge transfer (MLCT) through efficient dπ–pπ overlap (mainly to the *N*,*N*-diethylaminosalicylaldehyde unit) upon photochemical excitation, to the quenching in the blue-green channel. Upon Cu^{2+} chelation with **1**, opening of the lactam ring in the rhodamine unit was responsible for the pink-colored solution with a prominent absorption at 558 nm. The chelation process tended to switch the rhodamine unit to the oxidized form, thereby causing thermodynamically feasible π–d–π electronic coupling between the divalent Cu^{2+} ions and probe **1**. Upon photoexcitation, MLCT accompanied by PET from Cu^{2+} to the rhodamine unit through the diethylaminosalicylaldehyde unit in **1** resulted in quenching of the bluish-green emission centered at 480 nm along with the red channel. EPR and NMR spectroscopy revealed that the paramagnetic properties of **1C** existed solely upon complexation. DFT studies supported this hypothesis in terms of the HOMO and LUMO distributions and their relative band gap energies. The addition of PPi ions, however, selectively extruded the Cu^{2+} ions from the complex, resulting in a revival in fluorescence centered at 480 nm, along with reformation of the lactam ring, resulting in a colorless solution. **Scheme 2** provides a schematic representation of a plausible sensing mechanism.

(Scheme 2 will be added here)

miRNA Sensing

Taking advantage of the sequential colorimetric and fluorimetric changes in the recognition of Cu^{2+} and PPi ions in MeCN/H_2O (3:7, v/v%) at pH 7.0 (HEPES buffer), we initiated isothermal amplification of miRNA using a circular template. During the enzymatic (ϕ_{29} polymerase) amplification of miRNAs, PPi is generated through the consumption of dNTPs. Hence, we could track the enzymatically produced PPi analyte, recognized using a Cu^{2+} ensemble in modified ϕ_{29} buffer, at pH 7.5 [40 mM Tris-HCl, 50 mM $MgCl_2$, 50 mM KCl, 50 mM $(NH_4)_2SO_4$], in the presence of necessary supplements [1x BSA and dNTPs (2 mM each)]. Using this strategy eliminated any interference from pH-related factors, as well as any effects on the stability of the Cu^{2+} complex in the presence of thiols. DTT and 4-(1,1,3,3-Tetramethylbutyl)phenyl-polyethylene glycol (TRITON-X) are generally required for long-term storage of the buffered medium (they prevent cysteine oxidation via S–S bond formation, which can deactivate enzyme active sites), but not for biochemical catalysis [31]; thus, we were curious to modify the T4 ligase and ϕ_{29} buffer for miRNA recognition through the RCA process, especially if it could proceed within a shorter period of time.

When using a circular template for RCA, shorter circular oligonucleotides (generally 3–20 base pairs) are not suitable because additional steric hindrance and ring strain can result in less stable circular templates [32-34]. Thus, to gain high sensitivity along with high amplification efficiency (robustness), we used a 33-nt sequence having a circular template with 5´-phosphate modification to ligate with miRNA in the presence of T4 ligase at pH 7.5 in a buffer containing 50 mM Tris-HCl, 10 mM $MgCl_2$, 10 mM KCl, 10 mM $(NH_4)_2SO_4$, and 1 mM ATP (Table 1)[35,36].

With consideration of the enzyme active site's working pH as well as the thiol–thiolate interchange kinetics ($k = 3.3 \times 10^3$ M^{-1} min^{-1} at 30 °C), we set the pH of the T4 ligase buffer to 7.5 and applied specified salts and ATPs in 1x buffer [37]. To avoid the effects of dissolved oxygen, sterile and autoclaved DI H_2O was de-aerated for approximately 15 min, followed by the addition of the respective buffering chemicals for the preparation of the buffer. The phosphorylated 5´-end of the padlock probe came into close proximity with the 3´-OH unit in the presence of the perfectly matched miRNA-146a and was then ligated (duplex, 20 μL; T4 ligase, 5 μL; T4 buffer, 3 μL; H_2O, 2 μL; in a

30-μL reaction vessel) to form a circular template at 37 °C (method of inactivation of T4 ligase: heating at 65 °C for ca. 10 min).

To investigate the selectivity and sensitivity of our ensemble **1C** toward the padlock probe (5´-phosphorylated), we mixed miRNA-146a with various other miRNAs (Table 1) along with various mismatched (one-base, two-base, and sequence-variant) sequences. Polyacrylamide gel electrophoresis (PAGE) revealed high selectivity toward miRNA-146a, which was discriminated from various mismatched miRNA mixtures. Upon ligation with miRNA-146a and the padlock probe in the presence of T4 ligase, the resulting circular template forming a partial duplex with miRNA-146a would undergo amplification in the ϕ_{29} polymerase in the modified buffer solution containing 40 mM Tris-HCl, 50 mM $MgCl_2$, 50 mM KCl, and 50 mM $(NH_4)_2SO_4$ at pH 7.5 in deionized sterile H_2O along with an additional supplement (1x BSA) and dNTPs. Denaturing PAGE (18%) analysis validated the formation of a circular template in the presence of miRNA-146a, and that the RCA reaction proceeded in the presence of ϕ_{29} polymerase (2 μL) and dNTPs (12 μL) in a 20-μL RCA reaction vessel (Fig. 8).

We measured the EXO-I (Exonuclease I) activity to detect the circular template; this approach validated the formation of a stable ligated circular template. We monitored the EXO-I activity using the ligated circular DNA-RNA duplex (3 μL), EXO-I buffer (0.8 μL), EXO-I (1 μL), and sterile-DI H_2O (3.2 μL) in an 8-μL reaction vessel at 37 °C for 45 min. Termination of the reaction was performed by inactivating EXO-I at 75 °C for approximately 10 min.

(Figure 8 will be added here)

(Table 1 will be added here)

To determine the protocol for the rapid RCA reaction, after ligation in the presence of T4 ligase, the circular template was tested with different concentrations of the enzyme ϕ_{29} polymerase.

The ligation reaction was performed with T4 ligase (5 μL) and T4 ligase buffer (1x) by annealing the padlock probe (100 pM/μL) with miRNAs (100 pM/μL) at 85 °C within 10-15 min. and then incubated at 37 °C over 4-5 h. We then used the resulting circular probe for the isothermal amplification process with ϕ_{29} polymerase in the presence of 1x BSA. Upon increasing the enzyme content from 0.1 to 2 μL, the reaction rate increased, as revealed using an agarose gel; it was extremely fast within 20-25 min when using 2 μL of the enzyme per 20 μL of the RCA mixture.

We recorded UV-Vis and fluorescence spectra while maintaining a high amount of dNTPs (Figs. S21) to ensure significant optical changes in the presence of specified amounts of **1C**. The reaction rate was similar after adding 2 μL of the enzyme to 20 μL of the RCA reaction mixture under the modified buffered conditions. After various time intervals, the RCA reaction mixture was isolated and the ϕ_{29} polymerase deactivated by adding a quenching buffer containing 95% formamide/MeCN (pH 4.0, 5 μL); the mixtures were then analyzed through agarose gel electrophoresis (AGE). Within 30 min, an ssDNA of more than 10 kb was produced under the modified ϕ_{29} buffer conditions (Fig. 9). When we tried to increase the amount of ϕ_{29} polymerase under similar experimental conditions, the long-chain ssDNA product (10 kb < DNA gel) did not exhibit any significant changes within a shorter time interval. Accordingly, we varied the concentration of dNTPs (12, 10, 8, 6, 4, and 0 μL/20 μL) and monitored the signal amplification process. Based on the PPi consumption, we confirmed that PPi was generated during the RCA process. In addition, each set of RCA reaction mixtures was isolated and quenched after a specific interval of time (0, 2, 8, 16, 25, 37, 50, 80, 150, and 320 min) using the quenching buffer (5 μL). Thus, 20+5 μL of the RCA reaction mixture was used for the UV–Vis spectroscopic analysis with the **1C** ensemble in MeCN/H_2O (3:7, v/v%) at pH 7.0 (Fig. 10a). In the initial conditions and in the presence of RCA mixtures, the pH of the solution of **1C** was set at 6.0 (10 mM HEPES buffer). Nevertheless, after the addition of slightly basic RCA solution, the pH almost reached 7.0, as specified. The spectra of the RCA reaction mixtures obtained after various intervals exhibited concordant decreases in the intensity of the absorption peak at 558 nm, and became saturated after 50 min with complete extrusion of Cu^{2+} from the probe **1** through the effect of PPi.

When using 12, 10, or 8 μL of the dNTPs sample, saturation occurred after approximately 50 min, due to the excess production of PPi during signal amplification. In contrast, using 6 or 4 μL of the dNTPs produced an insufficient amount of PPi, resulting in partial revival of the clear solution. Notably, the colorimetric and fluorogenic responses of the probe **1** were not altered significantly in the presence of the various biologically relevant anions under the physiological conditions.

(Figure 9 will be added here)

When using the more highly sensitive fluorimetric method, the amount of dNTPs could be lowered by approximately 10 times, reaching a level that was appropriate for the concentration of Cu^{2+} ions. Accordingly, 2, 0.8, 0.6, 0.4, 0.2, and 0 μL of the dNTPs solution were used for the RCA reaction under the modified ϕ_{29} buffer conditions. Interestingly, greater than 70% of the quenched fluorescence was recovered within 20 min when using 2.0 or 0.8 μL of the dNTPs (Fig. 10b), confirming that the extrusion of Cu^{2+} ions was induced by the PPi produced from the RCA. We speculate that the PPi production that occurred after the incorporation of triphosphates was the prime reason for the revival of fluorescence, based on the presumably negligible decomposition of dNTPs in the buffer within the very short reaction interval (20–50 min).

Notably, the formation of gel from the RCA product was not observed in 2% AGE, but all of the padlock probe was consumed, supporting the consumption of the dNTPs during the miRNA-146a isothermal amplification process. These phenomena might also have been due to the extensive amount of ϕ_{29} polymerase, which could simultaneously produce various amplification cycles that resulted in a greater number of shorter chains. Notably, within the shorter time interval (ca. 6–7 min) of RCA, the reaction mixture was smeared throughout the AGE elution process (because the formation of multiple extensions and the incomplete consumption of dNTPs resulted in multiple bands), making it difficult to see the padlock sequence band. We attribute this smearing phenomenon to the excessive amount of ϕ_{29} polymerase, which simultaneously performed various amplification cycles and resulted in a greater number of shorter chains, rather than longer ssDNA fragments.

(Figure 10 will be added here)

The results above validated the successful extrusion of Cu^{2+} ions from **1C**, in a process related directly to the concentration of PPi ions produced during the amplification process. Notably, the concentration of Cu^{2+} ions with respect to PPi ions should be kept at a 1:2 ratio to obtain an appropriate colorimetric response (switching between the red and colorless solutions). Hence, the concentration of dNTPs in the RCA process should be recognizable in the presence of 2 μL of the enzyme ϕ_{29} polymerase.

The colorimetric and fluorimetric responses toward miRNA-146a were very selective in MeCN/H_2O (3:7, v/v%) at pH 7.0 (Figs. 11a and 11b). The interference effects observed for the padlock probe were negligible; even in the presence of various mixture of miRNAs [e.g., one- and two-base mismatches (ORN 1, ORN2)] or other miRNAs (miRNA-21), it did not display any significant changes in its optical response, confirming the highly selective nature of this system.

(Figure 11 will be added here)

To measure the sensitivity, we annealed 2 μL of the padlock probe and ligated it with various concentrations of miRNA-146a (diluted in DEPC buffer) in the presence of T4 ligase, followed by ϕ_{29} polymerase–aided isothermal amplification. After a 12-min interval, the RCA reactions performed with the various concentrations of miRNA-146a revealed lowest detection limits of 3.46 nM/μL (linear range from 1.7×10^{-10} to 4.12×10^{-6} M/μL) and 304.67 aM/μL (linear range from 1.20×10^{-20} to 9×10^{-15} M/μL) for the colorimetric and fluorimetric methods, respectively (Figs. 12 and 13). The obtained detection limits in the chromo-fluorogenic methods were good [38, 39]; we measured them in terms of three times the standard deviations with respect to the background signals, with negative control measurements.

While detecting the lowest detection response, initially we subjected various concentrations of miRNAs to the RCA process, which was calibrated using UV–Vis and fluorescence spectra (Figs. S22 and S23).

(Figure 12 and Figure 13 will be added here)

The colorimetric responses of the ensemble **1C** (25 μM) toward the RCA reaction mixtures containing various miRNAs were significant and could be distinguished clearly by the naked eye (Fig. 14).

(Figure 14 will be added here)

Thus, we have demonstrated miRNA-146a sensing and its amplification, determined with the aid of PPi recognition, using the selective and sensitive in situ-generated Cu^{2+} chromo-fluorescent ensemble **1C**, which undergoes a selective decomplexation process, under physiological conditions (Fig. 15). Notably, while detecting miRNAs in real samples (e.g., blood, spleen, tissues, cells, extracts), it would presumably always be preferable to remove any biological thiols and free radicals (e.g., $O_2^{\bullet}$, $NO^{\bullet}$) in preliminary steps (during the isolation process) to avoid interference. In addition, this technique provides a new approach for the real-time monitoring of nucleic acid amplification under specified conditions; we believe it is a much simpler and cheaper technology than the conventional real-time monitoring process. Although it has high selectivity, the sensitivity of this system might vary depending on the techniques used for handling the nucleic acids and their related proteins during their isolation and purification.

(Figure 15 will be added here)

Conclusion

We have developed a highly sensitive and robust method for miRNA sensing, and for monitoring its signal amplification, based on a label-free approach using the chromo-fluorescent Cu^{2+} ensemble **1C**. The sensing occurred through recognition of PPi ions produced during the signal amplification process, with selective extrusion of Cu^{2+} ions from the ensemble **1C** resulting in the red color (of **1C**) returning to colorless (for **1**) and with fluorescence appearing in the blueish-green channels. We attribute the higher selectivity and sensitivity of the divalent Cu^{2+}-based chromo-fluorogenic ensemble **1C** towards PPi in the RCA reaction mixture to the modified T4 ligase and ϕ_{29} buffer conditions providing an exceptionally high rate of amplification (>10 kb within 40-50 min) at elevated temperature (37 °C), thereby allowing miRNAs to be recognized very effectively under physiological conditions. Using this PPi sensing strategy, colorimetric and fluorimetric methods of miRNA-146a recognition reached nanomolar and attomolar levels of sensitivity, respectively, and high selectivity, without any optical instability under the modified buffer conditions (in the absence of DTT and TRITON-X). To the best of our knowledge, this report is the first to describe a label-free strategy for the recognition of universal miRNAs and for the monitoring of an isothermal amplification method when using a PPi sensing platform and Cu^{2+} ensembles, with both colorimetric and fluorimetric detection, under modified T4 ligase and ϕ_{29} buffered conditions.

Abbreviations

HEPES: 4-(2-hydroxyethyl)piperazine-1-ethanesulfonic acid

miRNA: microRNA

NMR: Nuclear magnetic resonance

piRNA: piwi-interacting RNA

mRNA: messenger RNA

RCA: Rolling circle amplification

FRET: Fluorescence resonance energy transfer

PPi: Pyrophosphate

MeOH: Methanol

MeCN: Acetonitrile

DMSO: Dimethyl sulfoxide

EDTA: Ethylenediaminetetraacetic acid

TRIS: Tris(hydroxymethyl)aminomethane

dNTPs: Deoxyribonucleotide triphosphates

ESI: Electrospray ionization

MLCT: Metal to ligand charge transfer

TRIZMA: TRIS buffer supplemented with NaCl and $MgCl_2$

DEPC: Diethyl pyrocarbonate

PAGE: Polyacrylamide gel electrophoresis

AGE: Agarose gel electrophoresis

TBE: Tris–boric acid–EDTA buffer

EB: Ethidium bromide

DTT: Dithiothreitol

TRITON-X: **4**-(1,1,3,3-Tetramethylbutyl)phenyl-polyethylene glycol

FTIR spectroscopy: Fourier transform infrared spectroscopy

EXO-I: Exonuclease I

HOMO: Highest occupied molecular orbitals

LUMO: Lowest unoccupied molecular orbitals

DFT: Density functional theory

PET: Photoinduced electron transfer

EPR: Electron paramagnetic resonance

ssDNA: Single stranded DNA

dsDNA: double stranded DNA

BSA: Bovine serum albumin

Associated Content and Supplementary Materials

Characterization data of the synthesized materials-NMR, mass, UV-Vis, and fluorescence spectroscopic data for probe **1**-are provided in the supplementary materials.

Notes

The authors declare no competing financial interest.

Acknowledgment

This study was supported by the National Research Foundation of the Republic of Korea (2017R1A2B4002398).

References

[1] A. S. Boutorine, D. S. Novopashina, O. A. Krasheninina, K. Nozeret, A. G. Venyaminova, Fluorescent probes for nucleic acid visualization in fixed and live cells, Molecules 18 (2013) 15357–15397.

[2] D.-L. Ma, H.-Z. He, K.-H. Leung, H.-J. Zhong, D. S.-H. Chan, C.-H. Leung, Label-free luminescent oligonucleotide-probes, Chem. Soc. Rev. 42 (2013) 3427–3440.

[3] X. Miao, Z. Cheng, H. Ma, Z. Li, N. Xue, P. Wang, Label-free platform for microRNA detection based on the fluorescence quenching of positively charged gold nanoparticles to silver nanoclusters, Anal. Chem. 90 (2018) 1098–1103. DOI: 10.1021/acs.analchem.7b01991.

[4] B. H. Le, Y. J. Seo, Highly sensitive miRNA-146a detection using gold nanoparticle based probing system and isothermal amplification, Anal. Chim. Acta 199 (2018) 155–160. https://doi.org/10.1016/j.aca.2017.11.016.

[5] C. S. Zhu, L. Zhu, D. A. Tan, X. Y. Qiu, C. Y. Liu, S. S. Xie, L. Y. Zhu, Avenues toward miRNA detections in vitro: A review of technical advances and challenges, Comput. Struct. Biotech. J. 17 (2019) 904–916. https://doi.org/10.1016/j.csbj.2019.06.018.

[6] Y. Xia, R. Zhang, Z. Wang, J. Tian, X. Chen, Recent advances in high-performance fluorescent and bioluminescent RNA imaging probes, Chem. Soc. Rev. 46 (2017) 2824–2843. doi:10.1039/c6cs00675b.

[7] Y. Cheng, L. Dong, J. Zhang, Y. Zhao, Z. Li, Recent advances in miRNA detection, Analyst 143 (2018) 1758–1774. DOI.10.1039/C7AN02001E.

[8] T. Tian, J. Wang, X. Zhou, A review: miRNA detection methods, Org. Biomol. Chem. 13 (2015) 2226–2238. DOI 10.1039/C4OB02104E.

[9] M. M. Ali, F. Li, Z. Zhang, K. Zhang, D.-K. Kang, J. A. Ankrum, X. C. Le, W. Zhao, Chem. Soc. Rev. 43 (2014) 3324–3341. DOI: 10.1039/c3cs60439j.

[10] W. Li, K. Ruan, MicroRNA detection by microarray, Anal. Bioanal. Chem. 394 (2009) 1117–1124. https://doi.org/10.1007/s00216-008-2570-2.

[11] M. de Planell-Saguer, M. C. Rodicio, Detection methods of miRNAs in clinical practice, Clin. Biochem. 46 (2013) 869–878. https://doi.org/10.1016/j.clinbiochem.2013.02.017.

[12] B. Schweitzer, S. Kingsmore, Combined nucleic acid amplification and detection, Curr. Opin. Biotechnol. 12 (2001) 21–27. https://doi.org/10.1016/S0958-1669(00)00172-5.

[13] B. K. Datta, S. Mukherjee, C. Kar, A. Ramesh, G. Das, Zn^{2+} and pyrophosphate sensing: Selective detection in physiological conditions and application in DNA-based estimation of bacterial cell numbers, Anal. Chem. 85 (2013) 8369–8375. dx.doi.org/10.1021/ac401871t.

[14] J. Qiang, C. Chang, Z. Zhu, T. Wei, W. Yu, F. Wang, J. Yin, Y. Wang, W. Zhang, J. Xie, X. Chen, A dinuclear copper(II) complex based sensor for pyrophosphate and its applications to detecting pyrophosphatase activity and monitoring polymerase chain reaction, Sens. Actuators B 233 (2016) 591–598.

[15] Z. Li, J. Qiang, J. Li, T. Wei, Z. Zhang, Y. Chen, Q. Kong, F. Wang, X. Chen, Di-nuclear Cu(II) complex bearing guanidinium arms for sensing pyrophosphate and monitoring the activity of PPase, Dyes Pigments 163 (2019) 243–248. https://doi.org/10.1016/j.snb.2016.04.082.

[16] H.-X. Jiang, Z.-Z. Liang, Y.-H. Ma, D.-M. Kong, Z.-Y. Hong, G-quadruplex fluorescent probe-mediated real-time rolling circle amplification strategy for highly sensitive microRNA detection, Anal. Chim. Acta 943 (2016) 114–122.

[17] H.-X. Jiang, M.-Y. Zhao, C.-D. Niu, D.-M. Kong, Real time monitoring of rolling circle amplification using aggregation induced emission, applications in biological detection, Chem. Commun. 51 (2015) 16518–16521.

[18] C. Niu, Q. Song, G. He, N. Na, J. Ouyang, Near infrared probes for bio applications based on silica coated gold nanopyramids with a distance dependent plasmon-enhanced fluorescence, Anal. Chem. 88 (2016) 11062–11069. https://doi.org/10.1021/acs.analchem.6b03034.

[21] R. Saba, D. L. Sorensen, S. A. Booth, MicroRNA-146a: A dominant, negative regulator of the innate immune response, Front. Immunol. 5 (2014) 578–589. DOI: 10.3389/fimmu.2014.00578.

[22] N. Rusca, S. Monticelli, miRNA-146a in immunity and disease, Mol. Biol. Intl. 2011 (2011) 437301. http://dx.doi.org/10.4061/2011/437301.

[23] P. Wolffs, H. Grage, O. Hagberg, P. Radstrom, Impact of DNA polymerases and their buffer systems on quantitative real-time PCR, J. Clinic. Microbiol. 42 (2004) 408–411. DOI: 10.1128/JCM.42.1.408-411.2004.

[24] E. Tenaglia, Y. Imaizumi, Y. Miyahara, C. Guiducci, Isothermal multiple displacement amplification of DNA templates in minimally buffered conditions using phi29 polymerase, Chem. Commun. 54 (2018), 2158–2161. DOI: 10.1039/c7cc09609g.

[25] R. C. Alexander, A. K. Johnson, J. A. Thorpe, T. Gevedon, S. M. Testa, Canonical nucleosides can be utilized by T4 DNA ligase as universal template bases at ligation junctions, Nucleic Acids Res. 31 (2003) 3208–3216. DOI: 10.1093/nar/gkg415.

[25] F. Tisato, C. Marzano, M. Porchia, M. Pellei, C. Santini, Copper in diseases and treatments and copper-based anticancer strategies, Med. Res. Rev. 30 (2010) 708–749. https://doi.org/10.1002/med.20174.

[26] M. G. Mohsen, E. T. Kool, The discovery of rolling circle amplification and rolling circle transcription, Acc. Chem. Res. 49 (2016) 2540–2550. https://doi.org/10.1021/acs.accounts.6b00417.

[27] K. Li, Y. Xiang, X. Wang, J. Li, R. Hu, A. Tong, B. Z. Tang, Reversible photochromic system based on rhodamine B salicylaldehyde hydrazone metal complex, J. Am. Chem. Soc. 136 (2014) 1643–1649. https://doi.org/10.1021/ja411689w.

[28] R. P. Sartoris, R. Calvo, R. C. Santana, O. R. Nascimento, M. Perec, R. F. Baggio, Structural and EPR studies of pyrophosphate-bridged dinuclear Cu^{II} complexes, Polyhedron 79 (2014) 178–185. http://dx.doi.org/10.1016/j.poly.2014.05.002.

[29] A. Pandith, K. R. Bhattarai, R. K. G. Siddappa, H.-J. Chae, Y. J. Seo, Novel fluorescent C_2-symmetric sequential *on-off-on* switch for Cu^{2+} and pyrophosphate and its application in monitoring of endogenous alkaline phosphatase activity, Sens. Actuators: B. Chem. 282 (2019) 730–742.

[30] E. Garribba, G. Micera, The determination of the geometry of Cu(II) complexes, J. Chem. Educ. 83 (2006) 1229–1232. https://pubs.acs.org/doi/pdf/10.1021/ed083p1229.

[31] S. Fjelstrup, M. B. Andersen, J. Thomsen, J. Wang, M. Stougaard, F. S. Pedersen, Y.-P. Ho, M. S. Hede, B. R. Knudsen, The effects of dithiothreitol on DNA Sensors 17 (2017) 1201-1210. https://doi.org/10.3390/s17061201.

[32] T. Povilaitis, G. Alzbutas, R. Sukackaite, J. Siurkus, R. Skirgaila, In vitro evolution of phi29 DNA polymerase using isothermal compartmentalized self replication technique, Protein Engineering, Design Selection 29 (2016) 617–628. https://doi.org/10.1093/protein/gzw052.

[33] D. Liu, S. L. Daubendiek, M. A. Zillman, K. Ryan, E. T. Kool, Rolling circle DNA synthesis: Small circular oligonucleotides as efficient template for DNA polymerase, J. Am. Chem. Soc. 118 (1996) 1587-1594. doi: 10.1021/ja952786k.

[34] L. Ulanovsky, M. Bodner, E. N. Trifonov, M. Choder, Curved DNA: Design, synthesis and circularization, Proc. Natl. Acad. Sci. USA 83 (1986) 862–866. https://doi.org/10.1073/pnas.83.4.862.

[35] M. Frieden, E. Pedroso, E. T. Kool, Tightening the belt on polymerases: Evaluating the physical constrains on enzyme substrate size, Angew. Chem. Int. Ed. 38 (1999) 3654–3657. https://doi.org/10.1002/(SICI)1521-3773(19991216)38:24%3C3654::AID-ANIE3654%3E3.0.CO;2-S

[36] E. M. Harcourt, E. T. Kool, Amplified miRNA detection by templated chemistry, Nucleic Acids Res. 40 (2012) e65. doi: 10.1093/nar/gkr1313.

[37] L. B. Poole, Basics thiols and cysteines in redox biology and chemistry, Free Radical Biol. Med. 80 (2014) 148–157. https://doi.org/10.1016/j.freeradbiomed.2014.11.013.

[38] M. Xiao, T. Man, C. Zhu, H. Pei, J. Shi, L. Li, X. Qu, X. Shen, J. Li, MoS_2 nanoprobe for miRNA quantifications based on duplex specific nuclease signal amplification, ACS Appl. Mat. Interfaces 10 (2018) 7852–7858. doi: 10.1021/acsami.7b18984.

[39] E. E. Augsperger, M. Rana, M. V. Yigit, Chemical and biological sensing using hybridization chain reactions, ACS Sensors 3 (2018) 878–902. https://doi.org/10.1021/acssensors.8b00208.

Schemes, Figures, and Table

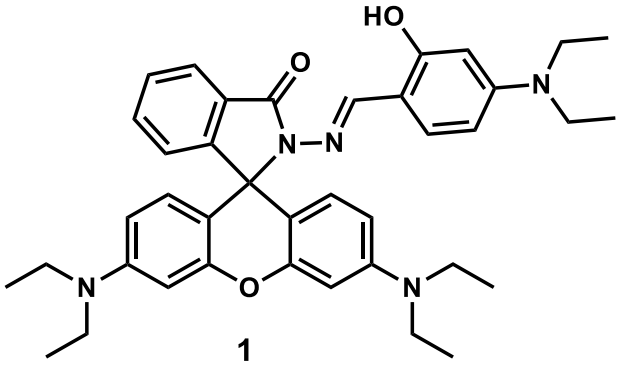

Scheme 1 Structure of the probe **1**.

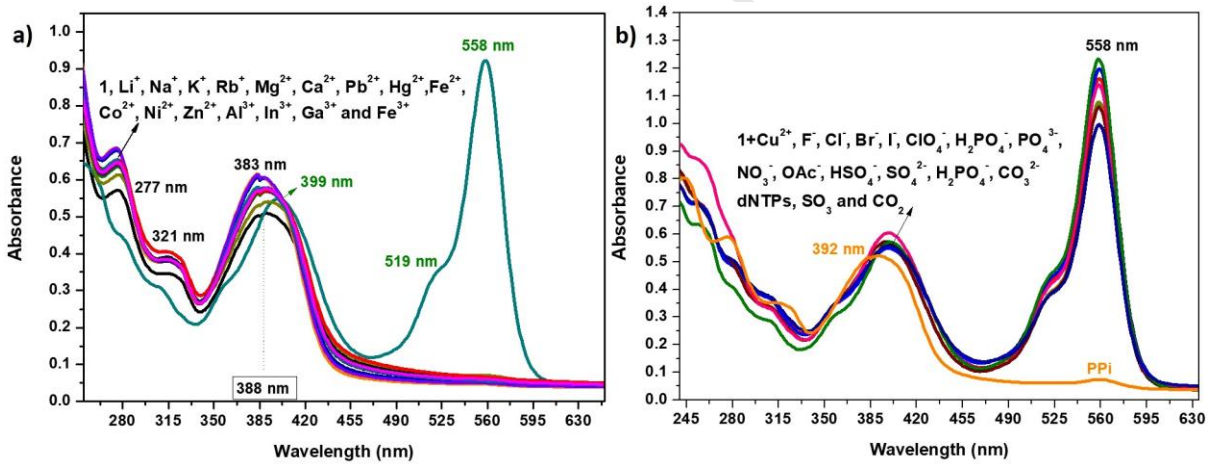

Fig. 1 a) UV–Vis spectra of the probe **1** (25 μM) in the absence and presence of metal ions (10.0 eq.) in MeCN/H_2O (3:7, v/v%) at pH 7.0 (HEPES buffer); b) UV–Vis spectra of the ensemble **1C** (25 μM) in the absence and presence of anions (25.0 eq.) in MeCN/H_2O (3:7, v/v%) at pH 7.0 (HEPES buffer). Each spectrum was recorded 20 min after the addition of the respective ions.

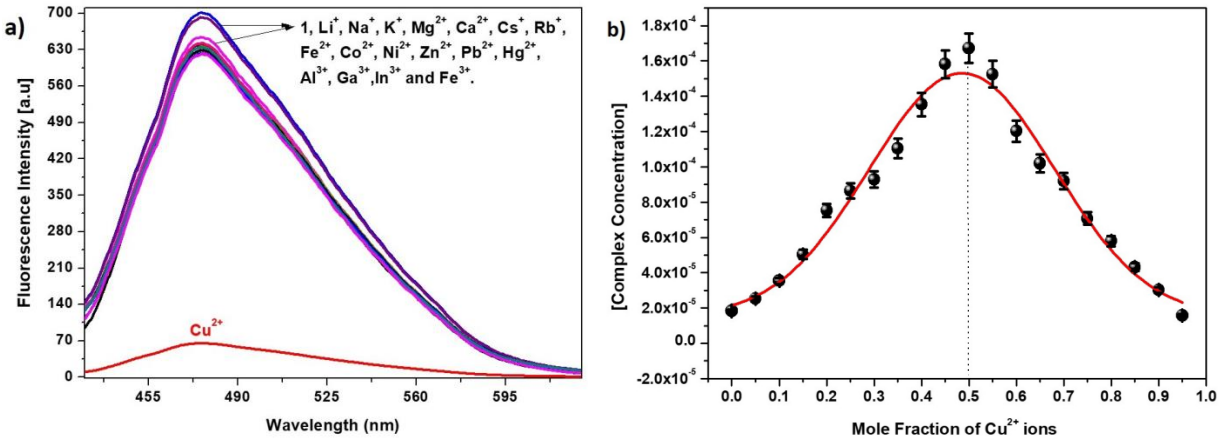

Fig. 2 a) Fluorescence spectra of the probe **1** (1 μM) and various metal cations (10.0 eq.). b) Job's plot of **1** (1 μM) with Cu^{2+} (1 μM) in MeCN/H_2O (3:7, v/v%) at pH 7.0 (HEPES buffer), upon excitation at (λ_{ex}) 402 nm; error range at (λ_{em}) 480 nm: <±6.87%. Note: In the Job's plot, the concentration of the complex is plotted with respect to the mole fraction of Cu^{2+} ions; the dependent variable is the change in emission intensity (ΔI) at 480 nm.

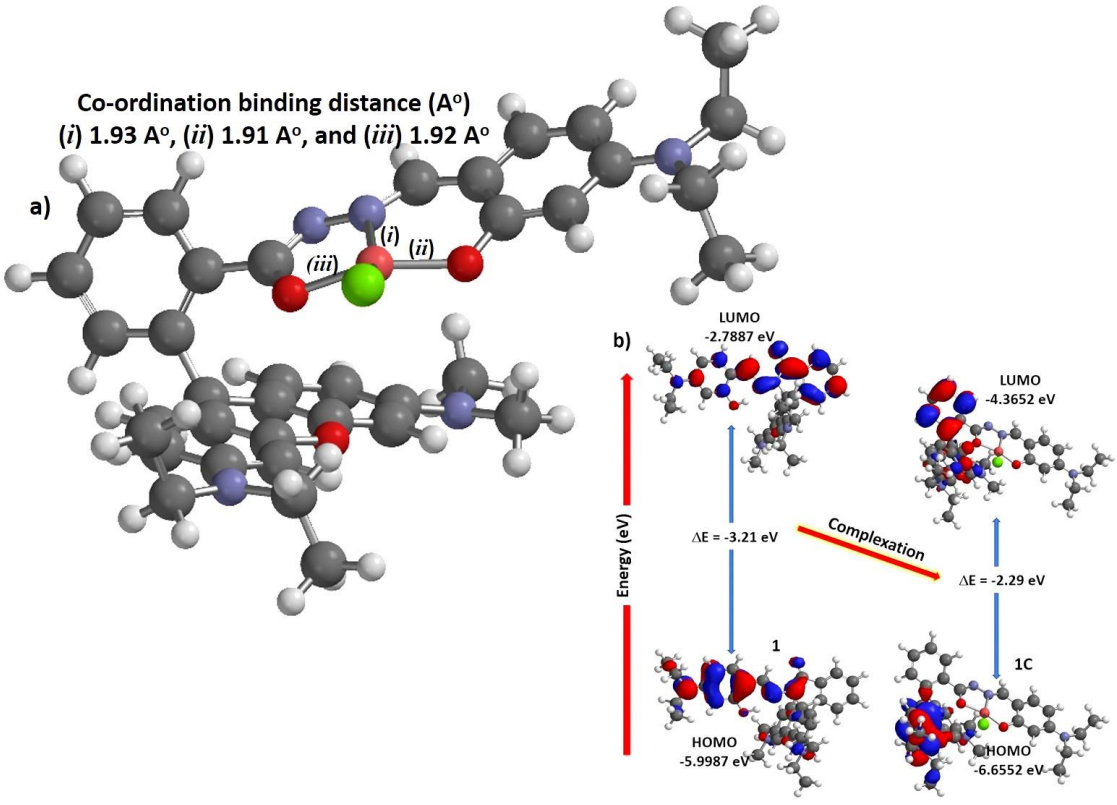

Fig. 3 a) DFT-based energy-minimized ground-state structure of the complex **1C** in H_2O as an implicit medium; b) HOMOs, LUMOs, and band gap energies (eV) calculated using the ωb97X-V/6-311+G(2df,p) basis set in H_2O as an implicit medium.

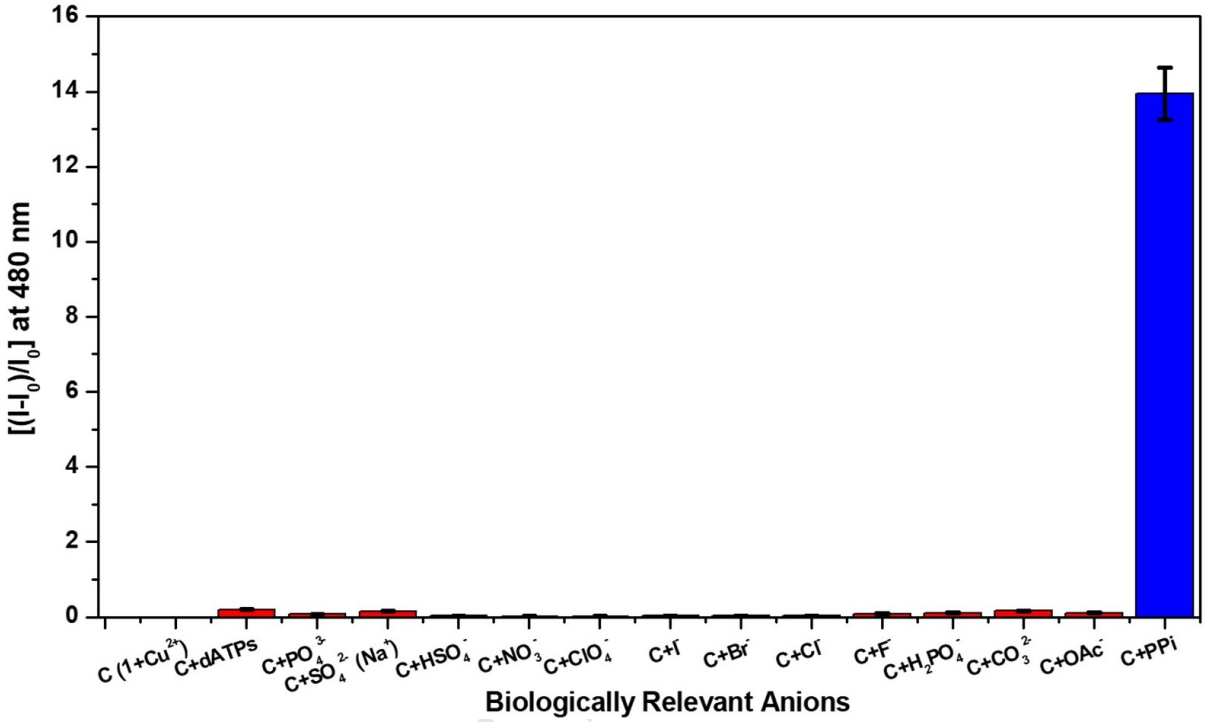

Fig. 4 Fluorescence intensity enhancement histogram [$(I - I_0)/I_0$] for a solution of **1C** (1 μM) in the presence of various anions (25 eq.) in MeCN/H_2O (3:7, v/v%) at pH 7.0 (HEPES buffer): λ_{ex} = 402 nm; λ_{em} = 480 nm. I_0 and I are the intensities of the ensemble **1C** at (λ_{em}) 480 nm in the absence and presence of anions, respectively. Error bars: <±5.56%.

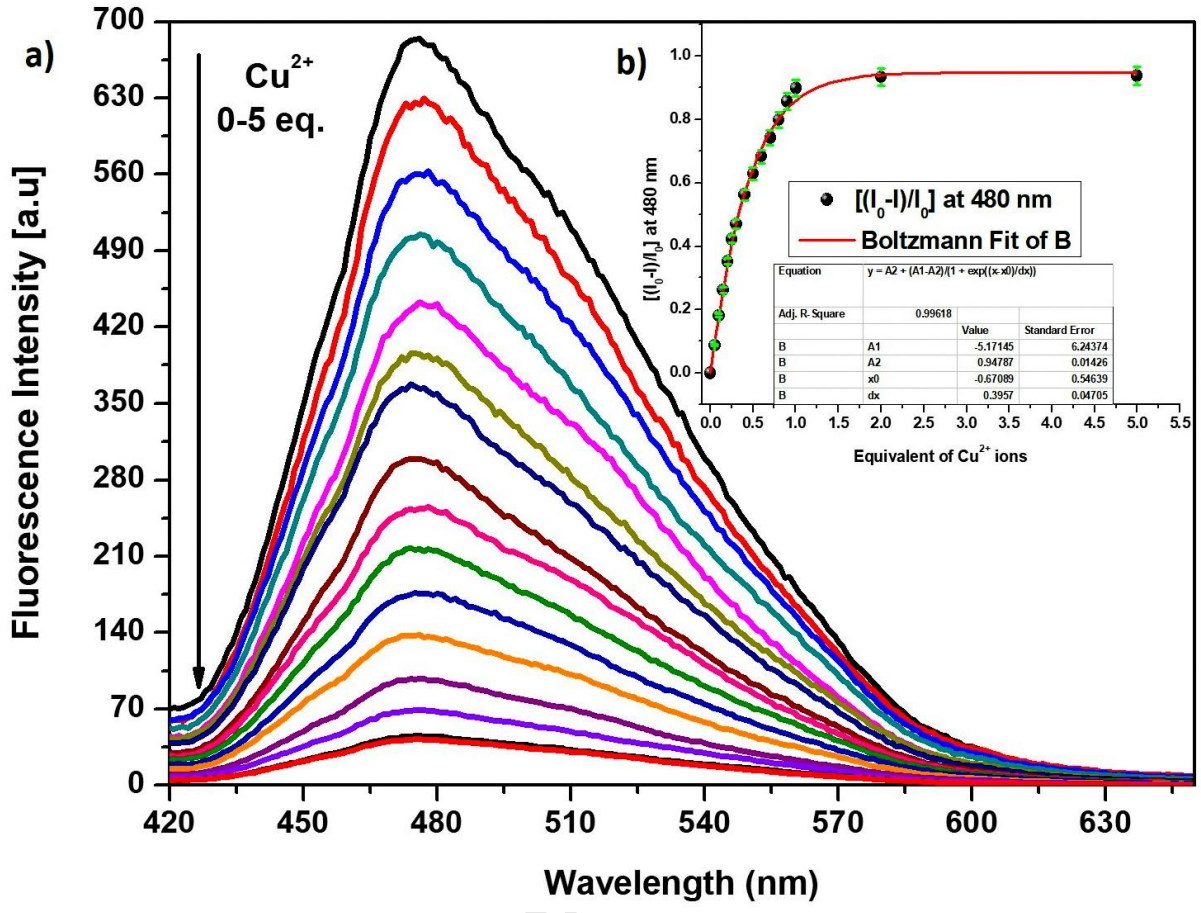
a)
Cu2+
0-5 eq.
Fluorescence Intensity [a.u]
Wavelength (nm)
b)
[(I0-I)/I0] at 480 nm
Boltzmann Fit of B
Equation y = A2 + (A1-A2)/(1 + exp((x-x0)/dx))
Adj. R-Square 0.99618
Value Standard Error
B A1 -5.17145 6.24374
B A2 0.94787 0.01426
B x0 -0.67089 0.54639
B dx 0.3957 0.04705
[(I0-I)/I0] at 480 nm
Equivalent of Cu2+ ions

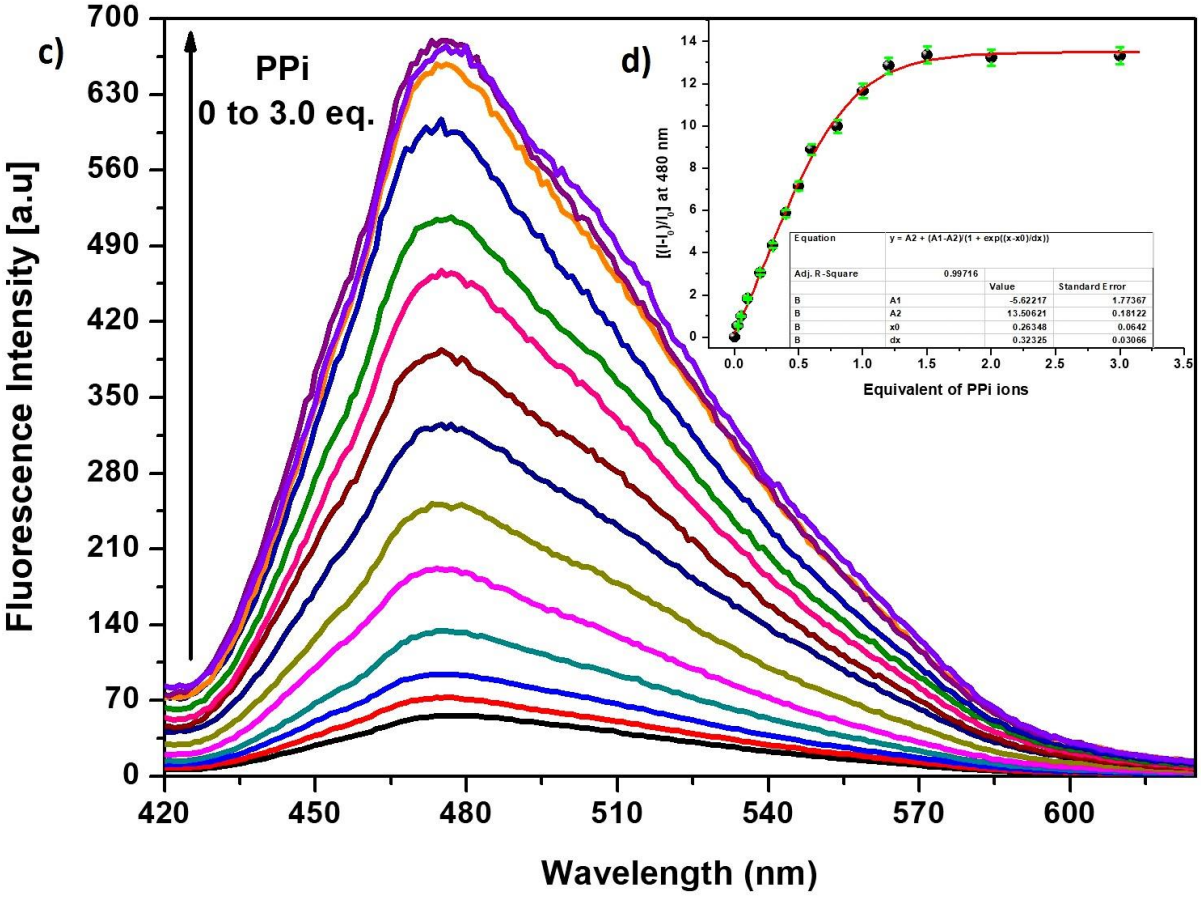
c)
PPi
0 to 3.0 eq.
Fluorescence Intensity [a.u]
Wavelength (nm)
d)
[(I-I0)/I0] at 480 nm
Equation y = A2 + (A1-A2)/(1 + exp((x-x0)/dx))
Adj. R-Square 0.99716
Value Standard Error
B A1 -5.62217 1.77367
B A2 13.50621 0.18122
B x0 0.26348 0.0642
B dx 0.32325 0.03066
Equivalent of PPi ions

Fig. 5 a) Fluorescence titration spectra of the probe **1** (1 μM) with Cu^{2+} ions (0–5.0 eq.) in MeCN/H_2O (3:7, v/v%) at pH 7.0 (HEPES buffer) at (λ_{ex}) 402 nm. Inset b) Intensity ratio [$(I_0 - I)/I_0$] plotted with respect to the number of equivalents of Cu^{2+} ions at (λ_{em}) 480 nm, where I_0 and I are the intensities of **1** in the absence and presence of Cu^{2+} ions, respectively. c) Fluorescence titration spectra of **1C** (1 μM) with PPi ions (0–3.0 eq.) in MeCN/H_2O (3:7, v/v%) at pH 7.0 (HEPES buffer) at (λ_{ex}) 402 nm. Inset d) Intensity ratio of **1C** [$(I - I_0)/I_0$] plotted with respect to the number of equivalents of PPi ions, where I and I_0 are the intensities of **1C** in the presence and absence of PPi ions, respectively. Note: While performing the titration with PPi, the emission intensity was stabilized after 10 min at ca. 1.5 μM of PPi; thereafter, the response toward the PPi ions was immediate.

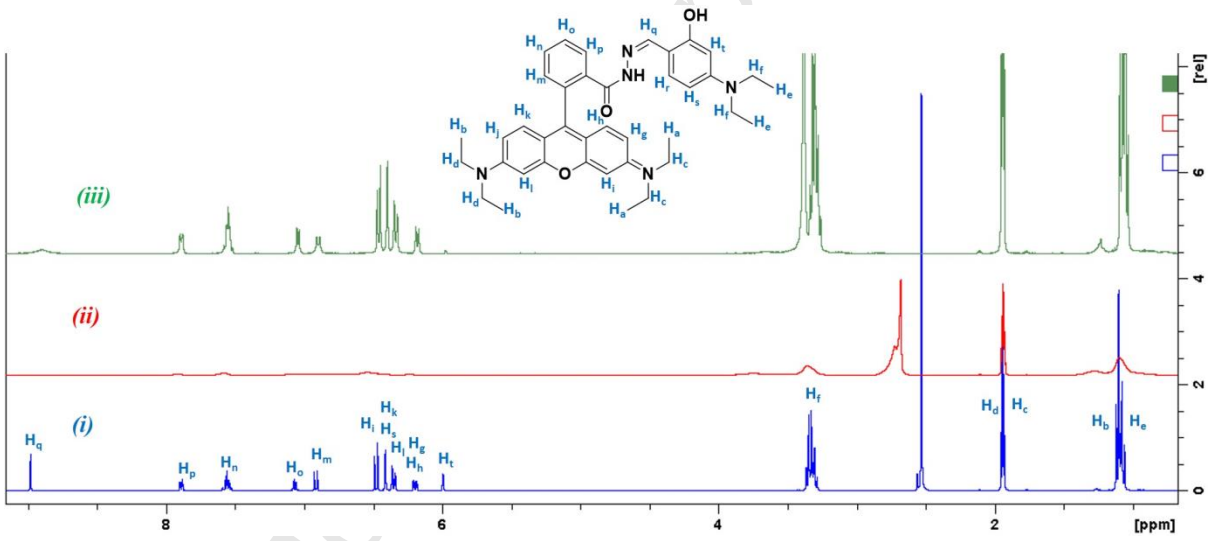

Fig. 6 Partial ^{1}H NMR spectra of i) **1** (1.5×10^{-3} M), ii) **1**●Cu^{2+} (1:1), and iii) **1**●Cu^{2+}+PPi (1:1:2) in CD_3CN/D_2O (7:3, v/v%).

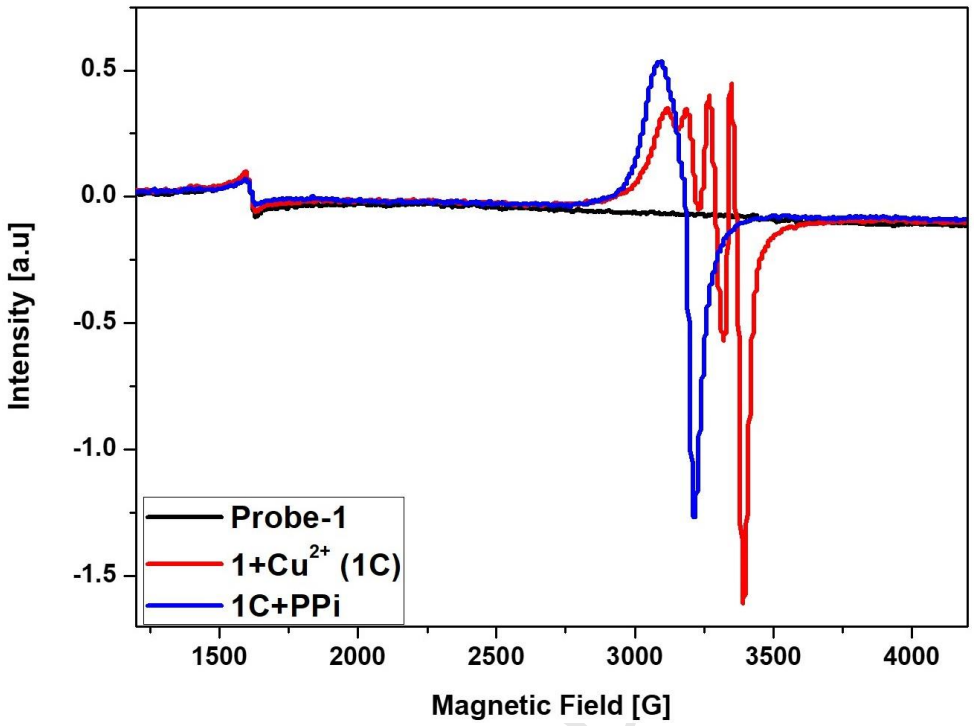

Fig. 7 EPR spectra of **1**, **1C** (1+Cu^{2+} 1:1), and **1C**+PPi in MeCN/H_2O (3:7, v/v%) at 298 K.

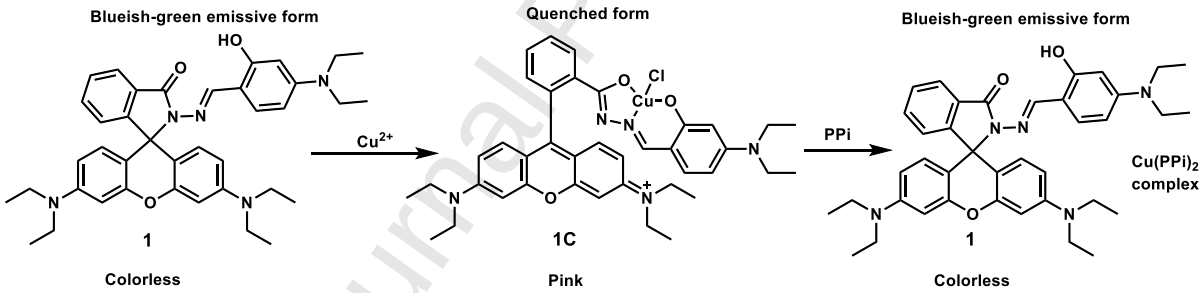

Scheme 2 Plausible mechanism of chromo-fluorogenic switching upon sequential additions of Cu^{2+} and PPi ions.

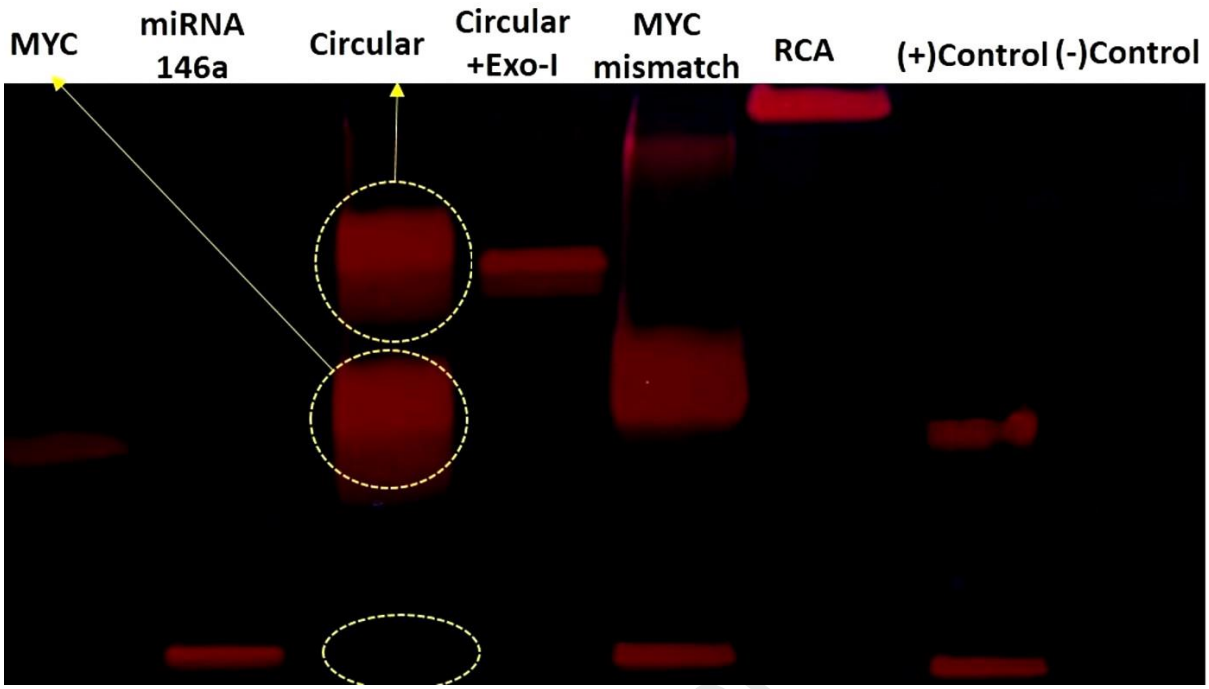

Fig. 8 Denaturing PAGE (18%) analysis of the RCA reaction monitoring process. First lane: template (padlock probe c-MYC); second lane: target, miRNA-146a; third lane: T4 ligase reaction circular; fourth lane: T4 ligase + EXO-I reaction Circular+EXO-I; fifth lane: padlock probe + miRNA21; sixth lane: RCA final product; seventh lane: (+)-control (c-MYC+miRNA-146a, only); eighth lane: (–)-control (blank). Note: In the (+)-control experiment, all of the components were present except for the T4 ligase and ϕ_{29} polymerase enzyme. Due to relative instability of miRNA's bands intensity were not high.

Table 1 Various oligonucleotide sequences tested (5´→3´)

Oligo/miRNA	Sequence (5´→3´)	Keynotes
Padlock probe	**P-5´**ATT CAG TTC TCA CCT CAG CCC TTC CCC ACC CTC CCC ACC CTC CCC ACC TCA GCA AAC CCA TGG A-3´	Green: complimentary to miRNA 146a
miRNA-146a	5´-UGA GAA CUG AAU UCC AUG GGU U-3´	Target analyte
miRNA-21	5´-UAG CUU AUC AGA CUG AUG UUG A-3´	Different miRNA
ORN 1	5´- UGA GAA CUG AAA UCC AUG GGU U -3´	One-base mismatch
ORN 2	5´- UGA GAA CUG AAA ACC AUG GGU U -3´	Two-base mismatches

ORN 3	5´- UGA GAA CGG AAA ACC AUG GGU U -3´	Three-base mismatches
ORN 4	5´- UGA GAA CUA AAU UCC AUG GGU U -3´	One-base mismatch
ORN 5	5´- UGA GAA CUA GAU UCC AUG GGU U -3´	Two-base mismatch

Note: Blue font represents the reverse complementary sequence of the c-MYC sequence; black sequence indicates the endonuclease nicking site; red font indicates the mismatches at the various position and bases.

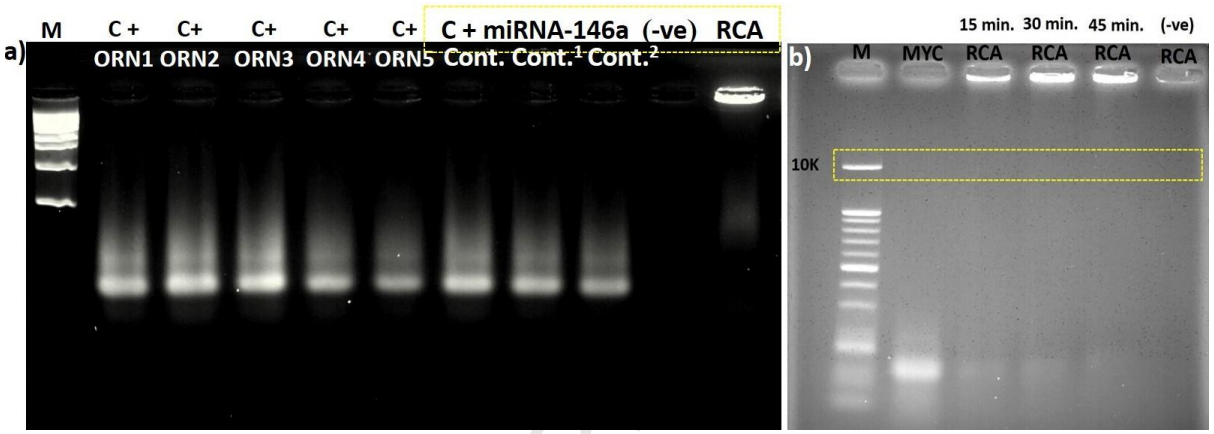

Fig. 9 a) 2% AGE studies of the template (c-MYC, noted as C after partial duplex formation) with various mismatched miRNAs (ORN1, ORN2, ORN3, ORN4, ORN5) in the reaction mixture, taken after the ligation and RCA steps. Note: "Cont." (circular duplex), "Cont.[1]," and "Cont.[2]" represent control experiments performed in the presence and absence of dNTPs and ϕ_{29}, respectively; "(-ve)" indicates the blank control. b) AGE (2%) of the circular-template RCA process after various time intervals in the presence of 2 μL of the enzyme ϕ_{29} (per 20 μL of RCA reaction mixture). Note: "M" represents the marker (1 kb/100 plus). To visualize the clear band at the bottom for the RCA products, a potential of 100 V was used for the AGE analysis.

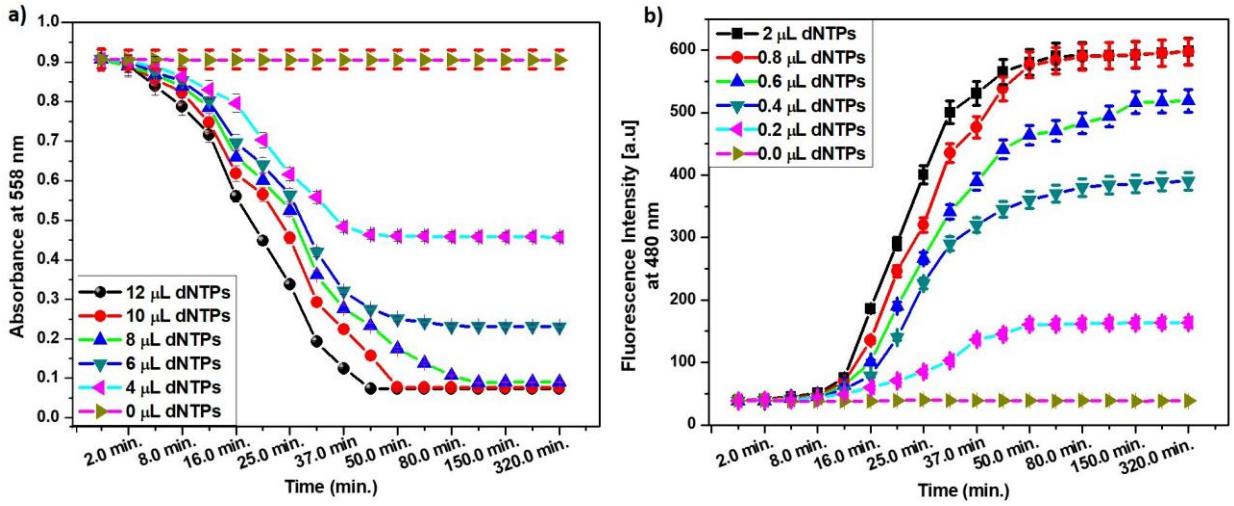

Fig. 10 a) Changes in UV–Vis spectral absorptivity at (λ_{max}) 558 nm for **1C** (25 μM) in RCA reaction mixtures containing various amounts of dNTPs in MeCN/H_2O (3:7, v/v%) at pH 7.0 (HEPES buffer). b) Fluorimetric changes recorded at (λ_{em}) 480 nm for **1C** (1 μM) in RCA reaction mixtures containing various amounts of dNTPs in MeCN/H_2O (3:7, v/v%) at pH 7.0 (HEPES buffer) upon excitation at 402 nm. Note: UV–Vis and fluorimetric spectral readings were taken from two different consecutive RCA reaction mixtures having different amounts of dNTPs, to validate the appropriate changes occurring in the presence of the ensemble **1C**. Each data point arose from three concordant readings with RSD <±1.56% (UV–Vis) and <±3.85% (fluorescence).

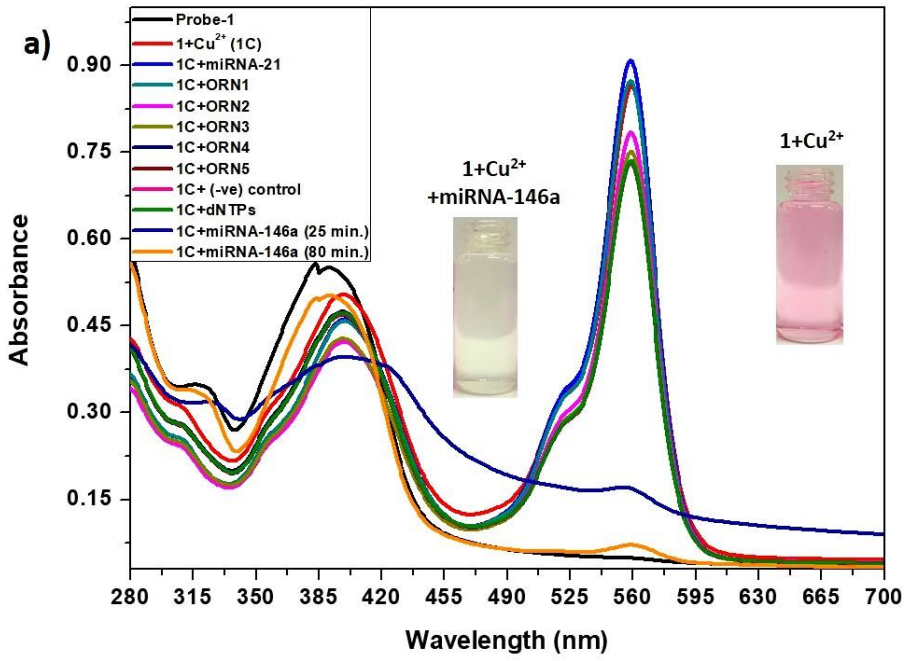

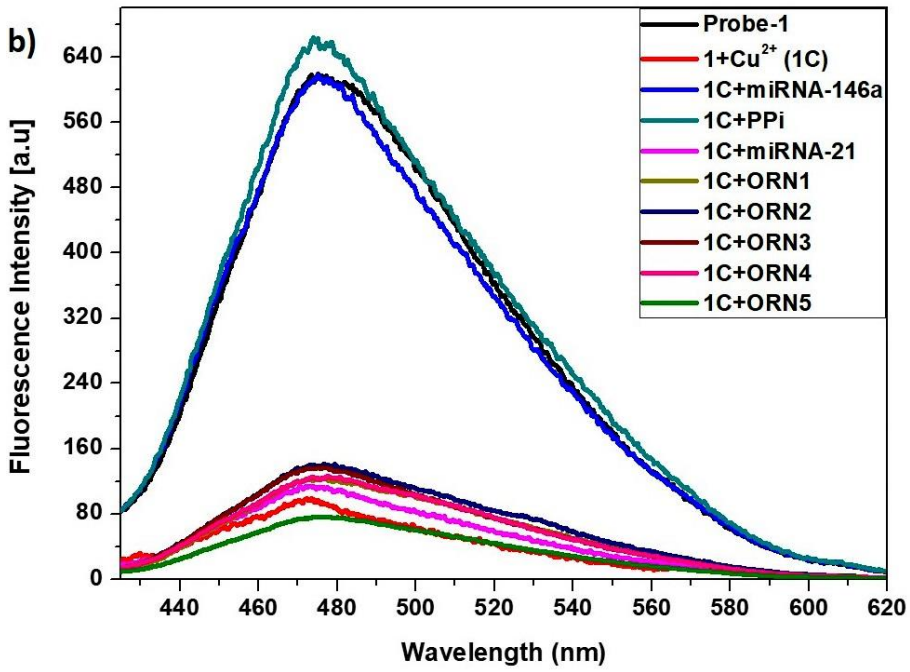

Fig. 11 a) UV–Vis spectra of a 25 μM solution of the ensemble **1C** and RCA reaction mixtures containing various miRNAs under the modified ϕ_{29} buffer conditions. b) Fluorescence spectra of a 1 μM solution of the ensemble **1C** in MeCN/H_2O (3:7, v/v%) at pH 7.0 (HEPES buffer).

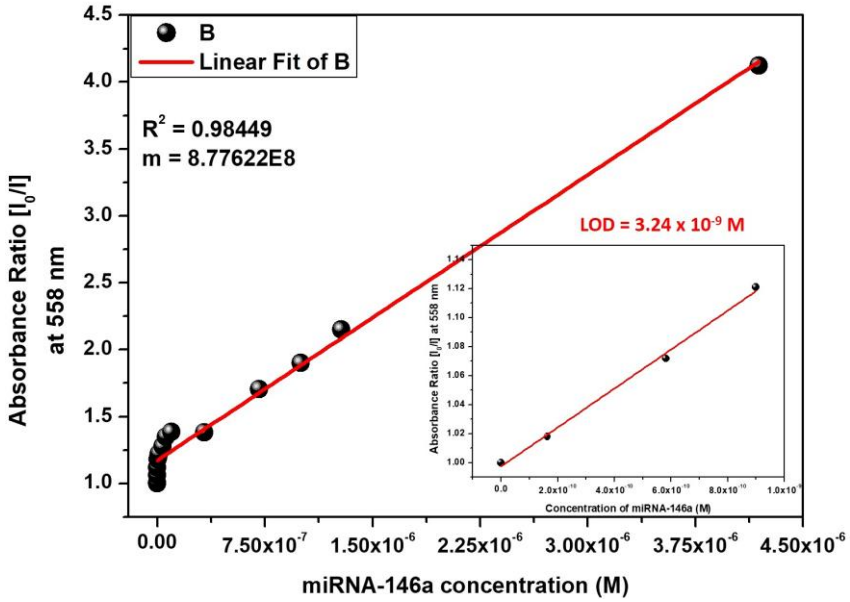

Fig. 12 Lowest colorimetric response of the ensemble **1C** (25 μM) toward miRNA-146a, in MeCN/H_2O (3:7, v/v%) at pH 7.0 (HEPES buffer), obtained through the RCA process within 12 min at 37 °C. Note: miRNA-146a was diluted in DEPC buffer and ligated in the presence of 10 μL of the padlock probe at 37 °C, followed by ϕ_{29}-aided amplification in the presence

of dNTPs (2 μL) and 1x BSA under the modified buffer conditions. Each data point was recorded after 12 min and calibrated with blank readings from samples containing only dNTPs, with a minimum of three readings.

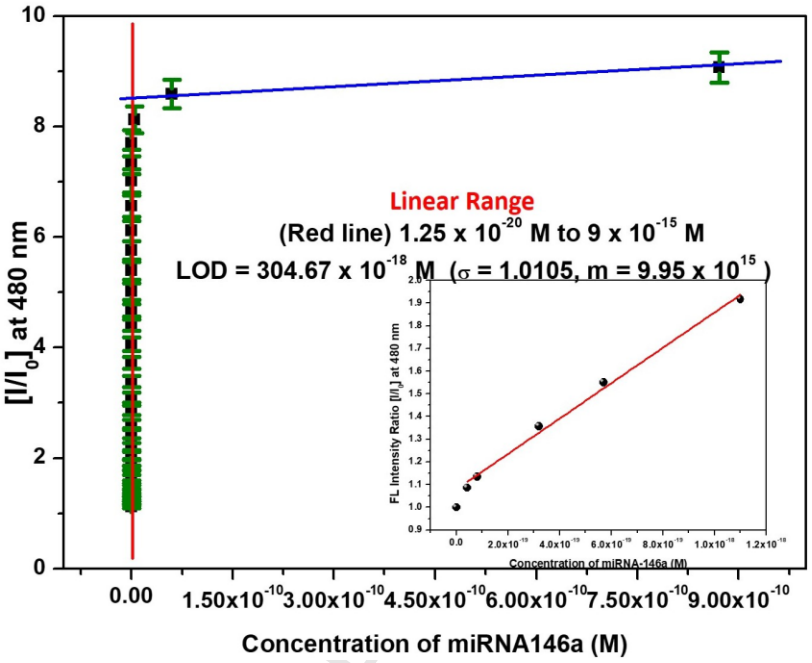

Fig. 13 Lowest fluorogenic response of the ensemble **1C** (1 μM) toward miRNA-146a, in MeCN/H_2O (3:7, v/v%) at pH 7.0 (HEPES buffer), obtained through the RCA process within 12 min at 37 °C. Inset: Enlarged portion of the zone for estimation of the LOD. Note: miRNA-146a was diluted in DEPC buffer and ligated in the presence of 10 μL of the padlock probe at 37 °C, followed by ϕ_{29}-aided amplification in the presence dNTPs (2 μL) and 1x BSA under the modified buffer conditions. λ_{ex} = 402 nm. Each data point was recorded after 12 min and calibrated with blank readings from samples containing only dNTPs. For clarity, only the lowest fluorogenic responses (a minimal number of data points) after the dynamic range are enlarged in the inset.

Fig. 14 a) UV–Vis colorimetric changes of a 25 μM solution of the ensemble **1C**. b) Fluorimetric changes of a 25 μM solution of the ensemble **1C** and the RCA reaction mixture in the presence of various miRNAs upon illumination at 365 nm (UV light). Note: Reaction mixtures were prepared using the standard protocol and collected after 80 min of ϕ_{29} polymerase extension under the modified buffered conditions. "+ve" Control: presence of miRNA-146a and enzyme only; "-ve" control: absence of miRNA-146a and enzyme.

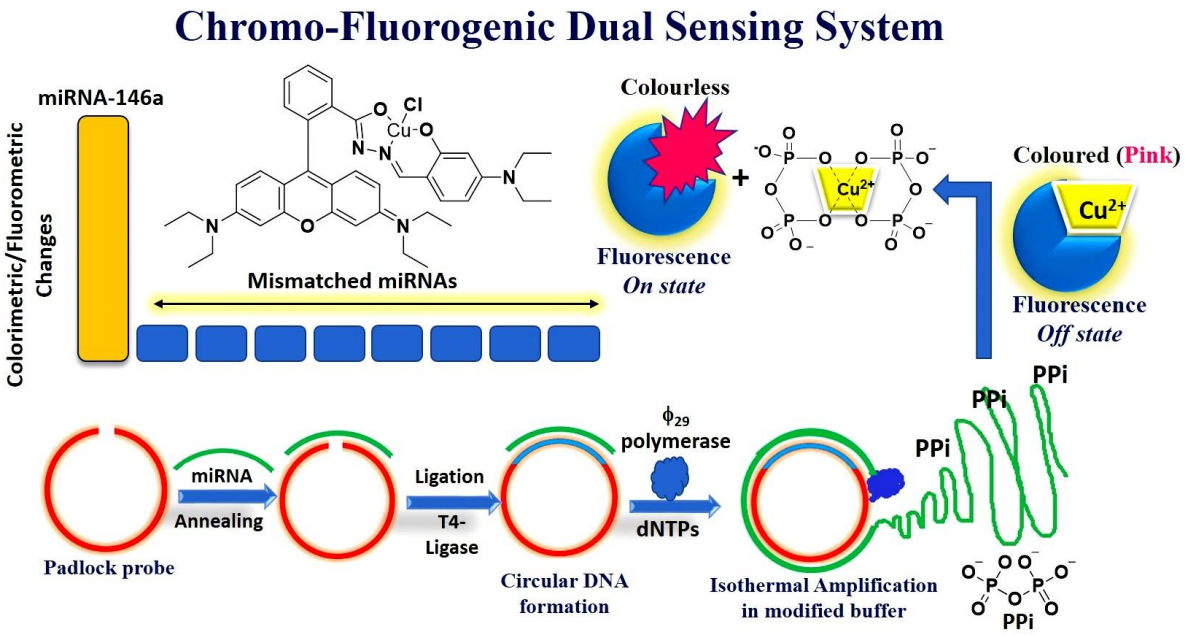

Fig. 15 Plausible sensing mechanism for miRNA-146a recognition.

Conflicts of Interest

Authors declare no conflicts of interest.

Graphical Abstract

Label-Free Sensing Platform for miRNA-146a Based on Chromo-Fluorogenic Pyrophosphate Recognition

Anup Pandith and Young Jun Seo*

Department of Chemistry, Chonbuk National University, Jeonju, 54398, Republic of Korea

Corresponding author: Tel.: +82 63 2703417; fax: +82. 63 2703408

E-mail: yseo@jbnu.ac.kr

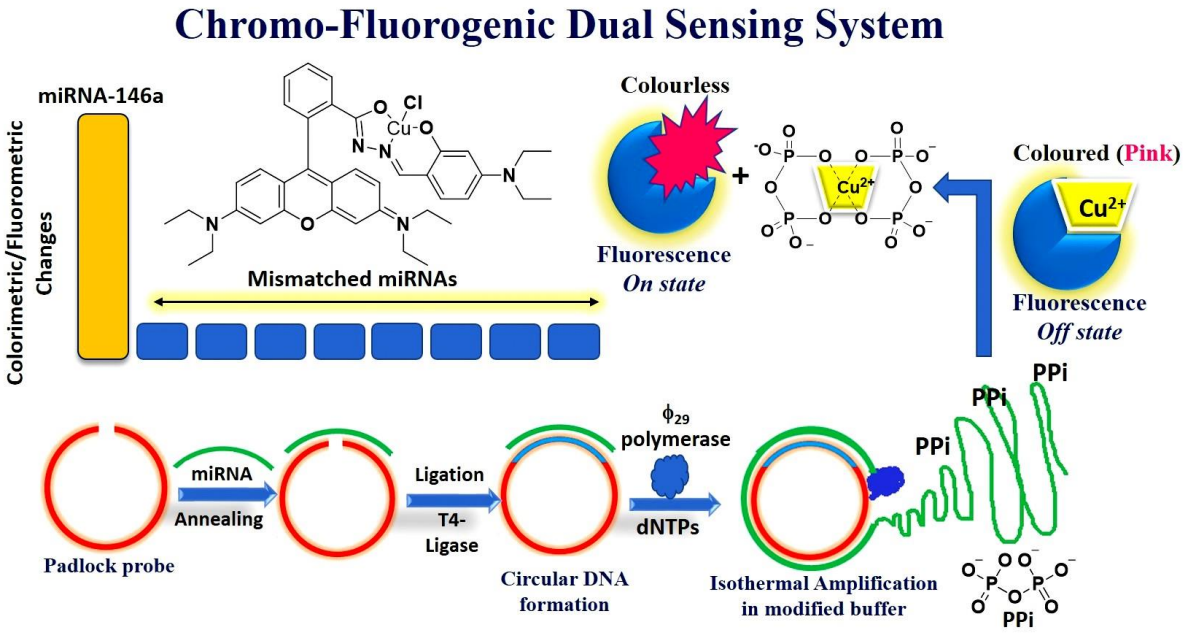

Cu^{2+} ensembles as an invitro-diagnostic tool: Robust and novel chromo-fluorogenic method for identification of miRNAs (up to nm and fM range) in modified biological buffers based on pyrophosphate sensing platform.

Highlights

- Chromo-fluorescent Cu^{2+} probe, for miRNA-146a recognition based on PPi sensing platform.
- Dual mode of miRNA's recognition in physiological conditions.
- Robust and real time monitoring of miRNA amplification in modified biological buffers.
- nM and aM level sensitivity towards miRNA in colorimetric and fluorometric methods.